

Neutron scattering investigations on methyl group dynamics in polymers.

Juan Colmenero^{1,2,3}, Angel J. Moreno¹, Angel Alegría^{2,3}

¹*Donostia International Physics Center, Paseo Manuel de Lardizabal 4, 20018 San Sebastián, Spain.*

²*Departamento de Física de Materiales, Universidad del País Vasco (UPV/EHU),
Apdo. 1072, 20080 San Sebastián, Spain.*

³*Unidad de Física de Materiales, Centro Mixto CSIC-UPV, Apdo. 1072, 20080 San Sebastián, Spain.*

Abstract

Among the different dynamical processes that take place in polymers, methyl group rotation is perhaps the simplest one, since all the relevant interactions on the methyl group can be condensed in an effective mean-field one-dimensional potential. Recent experimental neutron scattering results have stimulated a new revival of the interest on methyl group dynamics in glasses and polymer systems. The existence of quantum rotational tunnelling of methyl groups in polymers was expected for a long time but only very recently (1998), these processes have been directly observed by high-resolution neutron scattering techniques. This paper revises and summarizes the work done on this topic over last ten years by means of neutron scattering. It is shown that the results obtained in many chemically and structurally different polymers can be consistently described in the whole temperature range — from the quantum tunnelling limit to the classical hopping regime — as well as in the librational spectrum, in terms of the Rotation Rate Distribution Model (RRDM), which was first proposed in 1994. This model introduces a distribution of potential barriers for methyl group rotation, which is associated to the disorder present in any structural glass. The molecular and structural origin of the barrier distribution in polymers is discussed on the basis of a huge collection of investigations reported in the literature, including recent fully atomistic molecular dynamics simulations.

Keywords: Methyl groups; Quantum tunnelling; Classical hopping; Neutron scattering; Polymers.

Contents

I. Introduction

II. Neutron scattering techniques and instrumentation

IIA. Neutron scattering techniques

IIB. Neutron scattering instrumentation

IIC. Final experimental considerations

III. Methyl group dynamics in crystalline systems: Theory and scattering functions

IIIA. Rotational tunnelling

IIIB. Crossover from rotational tunnelling to classical hopping

IIIC. Classical hopping

IIID. Additional remarks

IV. Methyl group dynamics in polymer systems

IVA. Rotation Rate Distribution Model (RRDM)

IVB. Other approaches

V. Application of the RRDM to a showcase: poly(vinyl acetate)

VI. Summary of experimental results by neutron scattering on polymers

VIA. Classical hopping

VIB. Rotational tunnelling and crossover to hopping

VIC. Librational levels

VII. Molecular origin of the barrier distribution for methyl group dynamics

VIIA. Influence of the chain conformation

VII B. Influence of mixing with other materials

VII C. Molecular glasses and comparison with the crystalline state

VII D. Molecular dynamics simulations

VIII. Conclusions and outlook

Acknowledgements

References

Nomenclature

BS	Backscattering	A, E_a, E_b	Sublevels of the librational ground state
EISF	Elastic incoherent structure factor	$A(Q)$	Elastic incoherent structure factor
FEW	Fixed elastic window	B	Rotational constant
HWHM	Half-width at half-maximum	E_A	Classical activation energy
INS	Inelastic neutron scattering	$\langle E_A \rangle$	Average barrier of $f(E_A)$
MDS	Molecular dynamics simulations	E_{01}	First librational energy
NMR	Nuclear magnetic resonance	$F(E_{01})$	Distribution of E_{01}
QENS	Quasielastic neutron scattering	$f(E_A)$	Distribution of E_A
RRDM	Rotation Rate Distribution Model	$G(T_c)$	Distribution of T_c
TOF	Time of flight	$g(V_3)$	Distribution of V_3
VDOS	Vibrational density of states	$H(\log \Gamma)$	Distribution of $\log \Gamma$
		$h(\hbar\omega_t)$	Distribution of ω_t
		$I_{inc}(Q, t)$	Intermediate incoherent scattering function

$L(\omega, \Gamma)$	Normalized Lorentzian function
$\log \Gamma_0$	Average of $H(\log \Gamma)$
$S(Q)$	Elastic coherent structure factor
$S_{coh}(Q, \omega)$	Coherent scattering function
$S_{inc}(Q, \omega)$	Incoherent scattering function
$S_{inc}^{MG}(Q, \omega)$	Incoherent scattering function for methyl group rotation
T_c	Crossover temperature
V_3	Threefold barrier height
$\langle V_3 \rangle$	Average barrier of $g(V_3)$
W_3^c	Coupling potential between methyl groups
$Z(\omega)$	Generalized VDOS
$\hbar \mathbf{Q}$	Neutron momentum transfer
$\hbar \omega$	Neutron energy transfer
Γ	Lorentzian HWHM for classical hopping
Γ_{AE}	Inelastic crossover Lorentzian HWHM
γ_{AE}	Preexponential factor for Γ_{AE}
$\Gamma_{E_a E_b}$	Quasielastic crossover Lorentzian HWHM
$\gamma_{E_a E_b}$	Preexponential factor for $\Gamma_{E_a E_b}$
γ_b	RRDM preexponential factor for Γ_{AE} and $\Gamma_{E_a E_b}$
γ_s	RRDM preexponential factor for $\Delta\omega_t$
Γ_∞	Preexponential factor for classical hopping
$\Delta\omega_t$	Shift of the tunneling frequency
σ	Standard deviation of $H(\log \Gamma)$
σ_E	Standard deviation of $f(E_A)$
σ_V	Standard deviation of $g(V_3)$
σ_{coh}	Coherent cross-section
σ_{inc}	Incoherent cross-section
τ	Residence time for classical hopping
ω_t	Tunneling frequency
PC	Polycarbonate
PDMS	Poly(dimethyl siloxane)
PEO	Poly(ethylene oxide)
PEP	Poly(ethylene propylene)
PH	Phenoxy
PI	Polyisoprene
PIB	Polyisobutylene
PMMA	Poly(methyl methacrylate)
PMPS	Poly(methyl phenyl siloxane)
PP	Polypropylene
hh-PP	Head-to-head Poly(propylene)
PPO	Poly(propylene oxide)
PS	Polystyrene
PSF	Polysulfone
PVAc	Poly(vinyl acetate)
PVME	Poly(vinyl methyl ether)
P α MS	Poly(α -methylstyrene)
SCPE	Solution chlorinated polyethylene

I. INTRODUCTION

The different dynamic processes present in amorphous polymers cover a extremely wide time scale, spanning from ca. 10^{-13} s to years (see, e.g., Refs. [1–4]). These processes include terminal relaxations, conformational rearrangements, segmental dynamics, localized Johari-Goldstein relaxations, rotations of side groups, or fast vibrational dynamics. One of the simplest processes among the latter is methyl group, $-\text{CH}_3$, rotation. Many natural and synthetic macromolecular chains contain this simple molecular unit as a side group or as a part of more complicated side groups. In the glassy state of polymeric materials, at temperatures well below the glass transition region, one can assume as a good approximation that the main-chain dynamics are completely frozen-in and only small side units, as the methyl groups, can still remain mobile. In such conditions, the interaction between the methyl group and its environment is often well approximated by an effective mean-field or "single-particle" rotational potential [5–7]. The methyl group can be regarded as a rigid rotor because the strength of the C-H covalent bonds allows one to neglect the internal degrees of freedom in comparison with both translational and rotational motions of the group as a whole. Hence, the single-particle potential only depends on one characteristic angular coordinate ϕ , which is measured in the plane perpendicular to the C_3 -symmetry axis of the methyl group. The latter corresponds to the bond joining the carbon to the rest of the molecule (see Fig. 1).

In the simplest approximation (see Section III) the rotational potential is threefold:

$$V(\phi) = \frac{V_3}{2}(1 - \cos 3\phi). \quad (1)$$

Note that, in this form, V_3 corresponds to both the maximum and the amplitude of the potential $V(\phi)$. Figure 1 shows the quantized energy levels of a threefold potential with barrier height $V_3 = 500$ K (in the following V_3 will be given as V_3/k_B , with k_B the Boltzmann constant). Such levels are obtained [5–7] by solving the corresponding stationary Schrödinger equation, which in the case of a threefold potential takes the form of the well-known Mathieu equation (see, e.g., Ref. [8]). The energy levels $i = 0, 1, 2, \dots$ of the individual potential wells are named *torsional* or

librational levels, and are split (with energy splitting Δ_i) due to the coupling between the single-well wavefunctions. Three quantities characterizing the methyl group rotational potential are experimentally accessible (see below): i) the energies E_{0i} of the transitions between the librational levels, specially the transition E_{01} between the ground and first excited level, ii) the energy splitting of the ground librational state, $\Delta_0 = \hbar\omega_t$, with ω_t the quantum *tunnelling frequency*, iii) the activation energy E_A for methyl group classical hopping between adjacent wells, defined as the difference between the top of the barrier and the ground state (see Figure 1). The two former quantities can be directly accessed by inelastic spectroscopic techniques. The latter is indirectly derived from the temperature dependence of the hopping rate, which can be determined by quasielastic spectroscopy or by relaxation techniques (see below).

According to the scheme shown in Figure 1, methyl group dynamics at very low temperature (typically $T \lesssim 20$ K) is dominated by quantum rotational tunnelling, whereas classical hopping processes over the rotational barrier control the non-vibrational dynamics at high temperature (typically $T \gtrsim 80$ K). Due to the one-dimensional character of the rotational potential, methyl group dynamics is one of the simplest examples of barrier penetration phenomena involving the interaction of a quantum system with lattice vibrations. For that reason, it has attracted a great theoretical interest as an ideal case for the understanding of the fundamental problem of the transition from quantum tunnelling to classical hopping (see, e.g, Refs. [9–14]). Moreover, due to the high sensitivity of the rotational potential to the chemical and geometrical nature of the environment, and to the relative simplicity of their dynamics, methyl groups can be used as built-in probes for exploring structural and dynamic properties of the host material.

Dynamics, and in particular rotational tunnelling, of methyl groups has been widely investigated in molecular crystals by different techniques over last decades. (see, e.g., [5–7]). Measurements of tunnelling frequencies of methyl groups in about 200 systems of very different chemical nature have been compiled in Ref. [5]. The used techniques include mostly neutron scattering and nuclear magnetic resonance (NMR) methods (see, e.g., Ref. [15] for a review on NMR measurements), but also calorimetry, electron

nuclear double resonance, infrared or hole burning optical spectroscopy. However, no method yields such a direct model independent insight as inelastic neutron scattering (INS), where the tunnelling frequency is directly observed as two resolution-width inelastic peaks at $\pm\hbar\omega_t$. Nevertheless, it must be stressed that this observation is only possible for moderate and weak potentials ($V_3 \lesssim 700$ K). For stronger potentials $\hbar\omega_t$ is smaller than the current available instrumental resolution ($\approx 0.3 \mu\text{eV}$) and cannot be detected by neutron scattering spectroscopy. In such cases NMR is the mostly employed technique.

The lowest librational transitions E_{01} , E_{02} take values typically in the range 10–60 meV and can also be directly detected by INS as resolution-width inelastic peaks. However, they are observed in the same energy range that the other intramolecular vibrational modes and the lattice phonons. Though this fact often complicates the identification of methyl group librational transitions, measurements of the latter are useful for an accurate determination of the rotational potential, since as the tunnelling frequency, they strongly depend on the height and shape of the barrier.

Neutron scattering techniques have also been applied over the last decades to investigate methyl group dynamics in polymers. It is worth emphasizing that polymer systems are in general highly disordered materials. This implies that, in principle, one might expect the existence of a distribution of potential barriers for methyl group rotation, resulting from the different local environments present in the system. Indeed, the experimental librational peaks reported in the first INS investigations [16,17] in polymers showed a broad shape, as might be expected for an inherent distribution of potential barriers. However, this aspect of the problem, which had already been considered in NMR investigations [18,19], was ignored for a long time. Hence, first quasielastic neutron scattering data (QENS, see Section II) on classical hopping of methyl groups in polymers were analyzed, as for the case of crystalline systems, by assuming a unique value of the rotational potential. However, this procedure provided, in contrast to the result observed in crystalline systems, a non-Arrhenius temperature dependence of the hopping rate, and an apparent temperature dependence of the geometry of the motion, with large deviations from threefold rotation [20–26].

The presence of quantum tunnelling effects at un-

usually high temperature was considered as an unreliable explanation of the observed features, and a possible interpretation, by maintaining the picture of a unique rotational barrier, was discussed in terms of sixfold symmetry contributions to the rotational potential [20,21]. Another explanation was introduced in terms of temperature dependent fractions of rotating and non-rotating methyl groups [22,27]. Though a reasonable description of the experimental data was achieved, a physical justification of the latter hypothesis was lacking. Finally, it became clear that the basic assumption of a unique barrier was wrong for amorphous polymers when experiments on a same system performed in different spectrometers, i.e., in different time/energy windows, provided incompatible results for the measured hopping rate [23,24]. In the seminal works of Refs. [25] and [26], QENS data for methyl group hopping in polymers were successfully interpreted by introducing a broad distribution of rotational barriers, resulting from the highly disordered nature of the glassy state. In last years, a noticeable amount of experiments in different systems have supported this picture (see Sections V and VI).

Another aspect of the problem of methyl group dynamics in polymers is the dynamic behavior at very low temperature. From the early times, there was in the literature a number of claims or predictions about low temperature quantum effects. In particular, NMR measurements by Hoch *et al.* [28] showed methyl group dynamics in poly(vinyl acetate), PVAc, to be active down to very low temperature. Rotational tunnelling of methyl groups was also claimed to be present in poly(methyl methacrylate), PMMA, which would account for the reported non-Arrhenius behavior of the mechanical relaxation time at very low temperature [29,30]. However, a quantitative and unambiguous interpretation of the experimental data was not provided. As mentioned above, the rotational tunnelling picture has been evidenced in a vast collection of crystalline systems by different techniques, and specially by neutron scattering, where the tunnelling frequency is directly observed as two resolution-width inelastic peaks at $\pm\hbar\omega_t$. For the case of polymers, one might expect to observe broad peaks as a consequence of the distribution effects. However, observation of peaks, or of any scattered intensity over the instrumental resolution at very low temperature was not reported for a long time.

Finally, high resolution measurements in PVAc [31] and PMMA [32] at $T \approx 1$ K showed, instead of well-defined peaks, a broad scattered intensity similar to that commonly observed in the high temperature hopping regime. This result, which might have been interpreted as a signature of hopping events at unusually low temperature, was indeed explained in terms of *rotational tunnelling*, namely as the result of the presence of a strongly asymmetric distribution of tunnelling frequencies, with the maximum located well beneath the instrumental resolution. The latter distribution just followed from the distribution of potential barriers for methyl group rotation. This interpretation was supported by exploiting the expected isotope effect on the tunnelling frequencies [32] (see Section VI). The consistency of the distribution picture, formalized in the Rotation Rate Distribution Model (RRDM, see Section IV) was supported by the fact that the same barrier distribution was able to quantitatively account for the experimental spectra in all the temperature range [33,34], covering the crossover from rotational tunnelling to classical hopping, as well as the librational peaks observed by INS.

The grounds of the RRDM can, in principle, be extended to non-polymeric disordered systems, as has been successfully checked in the glassy state of toluene [35] and sodium acetate trihydrate [36] (see Section VII). Contrary to the case of polymer systems, results for methyl group dynamics in molecular glasses can be directly compared with those for the crystalline state, allowing one to get insight into the molecular origin of the barrier distribution.

The goal of this review is to summarize the progress in the topic of methyl group dynamics in polymers that has been achieved over last 10 years by means of neutron scattering techniques, together with the development of the RRDM. The molecular origin of the distribution of potential barriers, which is an essential ingredient of the RRDM, is discussed on the basis of the experimental and computational investigations reported in the literature. A brief introduction to the theoretical and experimental grounds of neutron scattering techniques is also given in next Section.

II. NEUTRON SCATTERING TECHNIQUES AND INSTRUMENTATION

A. Neutron scattering techniques

Neutrons are adequate probes for the investigation of both structure and dynamics of condensed matter. There are three major features for that: i) their typical wavelengths are of a few Å, which correspond to the typical interatomic distance, ii) their typical energies are of the order of some meV, which correspond to the energy scale of the typical excitations in condensed matter, iii) neutrons being particles without electrical charge, they can penetrate the sample and provide information about bulk properties, in contrast to charged particles like electrons, which mainly probe surface properties.

The range of the nucleus-neutron interaction is $\sim 1.5 \times 10^{-5}$ Å, much smaller than the neutron wavelength and the nuclear radius. Hence, scattering can be approximated as isotropic, and the interaction is modelled by the Fermi pseudopotential:

$$V_F = \frac{2\pi\hbar^2}{m} b \delta(\mathbf{r} - \mathbf{R}), \quad (2)$$

where m and \mathbf{r} are respectively the neutron mass and position, and \mathbf{R} is the nucleus position. The scattering length operator, b , is given by

$$b = b_{coh} + \frac{2b_{inc}}{\sqrt{I(I+1)}} \mathbf{S} \cdot \mathbf{I}, \quad (3)$$

where \mathbf{S} and \mathbf{I} are respectively the neutron and nuclear spins, and b_{coh} and b_{inc} are respectively the coherent and incoherent scattering lengths.

As in any scattering technique, there are two basic quantities to be measured by neutron scattering: the energy transfer, $\hbar\omega = \hbar^2(k^2 - k_0^2)/2m$, which is the difference between the final and the initial neutron energy, and the momentum transfer, $\hbar\mathbf{Q} = \hbar\mathbf{k} - \hbar\mathbf{k}_0$, where \mathbf{k} and \mathbf{k}_0 are respectively the final and initial neutron wavevectors (see Fig. 2). The number of neutrons scattered within a solid angle between Ω and $\Omega + d\Omega$, which have changed their energy in $\hbar\omega$ and their momentum in $\hbar\mathbf{Q}$, is proportional to the double-differential cross-section [37–40]. The latter can be split in two parts, the coherent and the incoherent double-differential cross-sections:

$$\frac{\partial^2 \sigma}{\partial \Omega \partial \omega} = \left(\frac{\partial^2 \sigma}{\partial \Omega \partial \omega} \right)_{coh} + \left(\frac{\partial^2 \sigma}{\partial \Omega \partial \omega} \right)_{inc}, \quad (4)$$

which can be expressed as a function of the scattering functions:

$$\begin{aligned} \left(\frac{\partial^2 \sigma}{\partial \Omega \partial \omega} \right)_{coh} &\propto \frac{k}{k_0} \sigma_{coh} S_{coh}(Q, \omega) \\ \left(\frac{\partial^2 \sigma}{\partial \Omega \partial \omega} \right)_{inc} &\propto \frac{k}{k_0} \sigma_{inc} S_{inc}(Q, \omega). \end{aligned} \quad (5)$$

In this equation σ_{coh} and σ_{inc} are respectively the coherent and incoherent cross-sections. $S_{coh}(Q, \omega)$ and $S_{inc}(Q, \omega)$ are respectively the coherent and incoherent scattering functions. These functions give account for the amplitude transitions, mediated by the Fermi pseudopotential, between the eigenstates of the sample. While the coherent contribution results from interferences between the neutron waves dispersed by the nuclei, the incoherent contribution is equivalent to the dispersion of the isolated nuclei. In the classical limit, $S_{coh}(Q, \omega)$ and $S_{inc}(Q, \omega)$ are related via double Fourier transform, respectively, with the pair-correlation and self-correlation functions of the atomic positions.

Protium hydrogen (H) has a large incoherent scattering cross-section as compared to its coherent part and to the total cross-section, $\sigma_{tot} = \sigma_{inc} + \sigma_{coh}$, of the other elements typically present in polymer materials (see Table I). Hence, a neutron scattering experiment on a protonated polymer sample provides mainly information on the self-correlation function of the protium hydrogens. Moreover, due to the large difference between the incoherent cross-section of protium and the total cross-section of deuterium (D), the intensity scattered by a subset of the protium hydrogens can be strongly enhanced if selective deuteration of the other hydrogens is possible by means of chemical methods.

When neutron scattering is used for dynamic investigations, one finds three different types of scattering processes: elastic, quasielastic and inelastic scattering. Inelastic neutron scattering (INS) corresponds to the case where the neutron exchanges energy with the sample excitations, and manifests in the experimental spectrum as two resolution-width lines of finite energy (for neutron energy gain and loss). On the contrary, elastic scattering corresponds to the case where the neutron energy remains constant, yielding a resolution-width elastic line. Finally, quasielastic neu-

neutron scattering (QENS) is that associated with the energy transfer resulting from the Doppler effect occurring when a neutron interacts elastically with a moving particle, and manifests as a broad line around the elastic line. Of course, inelastic or quasielastic processes are not detectable when the involved energy change is smaller than the instrumental energy resolution, yielding an additional contribution to the experimental elastic line. Quasielastic and inelastic processes typically cover a range $|\hbar\omega| < 2$ meV and $|\hbar\omega| > 2$ meV respectively, the latter corresponding to typical vibrational excitations in condensed matter. The terms QENS and INS are often used to refer to these energy ranges and the dynamic window of the corresponding spectrometers. However, it must be stressed that excitations in the μeV range can also be present in the system, as the case of methyl group tunnelling. Hence, such excitations, which strictly correspond to INS, are accessible by means of instruments specifically designed for QENS.

In the liquid state, molecules are able to diffuse and lose memory from their initial positions. Molecular diffusion yields no elastic component in neutron scattering spectra. On the contrary, if the motion of a group of particles is constrained into a localized region, as the case of methyl group rotation in a crystalline or glassy system, in addition to the eventual inelastic and quasielastic contributions, such a motion provides an elastic component in the experimental spectrum. The elastic peak is modulated by a Q -dependent quantity named the elastic-incoherent-structure-factor (EISF), $A(Q)$. The EISF gives account, via Fourier transform, for the average positions of the individual particles performing the localized motion, i.e., it provides information about the geometry of the motion.

Integration of the coherent scattering function provides the elastic coherent structure factor, $S(Q)$. Fourier transformation of the latter gives account for the probability distribution of the configurations of all the ensemble of particles in the system, i.e., it provides static structural information.

B. Neutron scattering instrumentation

Neutron scattering investigations on methyl group dynamics in polymers are carried out mainly by means of time-of-flight (TOF) and high-resolution backscat-

tering (BS) techniques. In addition, in most of the cases it is convenient to evaluate the total coherent and incoherent contributions to the scattered intensity. For this purpose, diffraction experiments with spin polarization analysis are necessary. The showcase presented here for PVAc (see Section V) corresponds to experiments performed at the spectrometers IN5, IN6, IN16 and D7 of the Institut Laue Langevin, (ILL, Grenoble, France) and TOSCA at the source ISIS of the Rutherford Appleton Laboratory (RAL, Chilton, United Kingdom). Next we summarize the technical characteristics of these spectrometers. A detailed description can be found in Refs. [41–46].

IN5 [41] and IN6 [42] are TOF spectrometers. By means of a monochromator, different wavelengths, λ , can be selected in the ranges 1.8–16 Å for IN5 and 4–6 Å for IN6. Most of the data presented here were obtained with $\lambda = 6.5$ Å at IN5 and $\lambda = 5.1$ Å at IN6. In this situation the elastic energy resolution (half-width at half maximum, HWHM) is ≈ 25 μeV for IN5 and ≈ 50 μeV for IN6. The explored energy window (in neutron energy gain) is -0.6 meV $\lesssim \hbar\omega \lesssim 19.5$ meV for IN5, and -2 meV $\lesssim \hbar\omega \lesssim 1600$ meV for IN6. The scattering function $S(Q, \omega)$ at constant Q can be obtained from the experimental quantity which is directly measured, namely $S(\Phi, \omega)$, where Φ is the scattering angle, by an interpolation procedure according to the trivial geometrical relation:

$$\hbar^2 Q^2 / 2m = 2E_0 + \hbar\omega - 2\sqrt{E_0(E_0 + \hbar\omega)} \cos \Phi, \quad (6)$$

where m is the neutron mass and $E_0 = \hbar^2 k_0^2 / 2m$ is the incoming neutron energy. The interpolation procedure provides reliable spectra in the quasielastic energy range $|\hbar\omega| \lesssim 2$ meV for a Q -range of $0.6 \text{ \AA}^{-1} \lesssim Q \lesssim 1.8 \text{ \AA}^{-1}$, both ranges being of interest for investigations on methyl group rotation.

IN5 and IN6 are suitable to investigate methyl group rotational hopping at intermediate and high temperature, where the corresponding time scale is typically of the order of 10 ps, but usually are not adequate for the investigation of rotational tunnelling. Only when the rotational barrier is very low ($V_3 \lesssim 200\text{K}$) the tunnelling lines are accessible in the energy range covered by TOF spectrometers. For higher barriers, the use of backscattering instruments is needed.

IN16 is a high-resolution BS spectrometer [43] which can explore excitations in the μeV -range, and correspondingly, time scales of the order of 1 ns. The high

resolution of IN16 makes it adequate for the investigation of methyl group dynamics in, both, the classical hopping regime at intermediate temperature, and the quantum tunnelling regime at very low temperature. By using a Si (111) monochromator the wavelength of the incident neutrons is $\lambda = 6.27 \text{ \AA}$. The corresponding accessible Q -range is $0.2 - 1.9 \text{ \AA}^{-1}$. When deformed Si (111) crystals are used as analyzers a resolution of nearly Gaussian shape with HWHM $\approx 0.45 \mu\text{eV}$ is attained. In the standard operation mode the monochromator is subject to an oscillatory motion at a frequency of $\approx 14 \text{ Hz}$, which allows one to explore an energy transfer range up to $15 \mu\text{eV}$. As in backscattering spectrometers the incoming beam energy is much larger than the maximum energy transfer, Eq. (6) can be approximated by a direct relation between the position of the detector and the momentum transfer, given by:

$$Q = (4\pi/\lambda) \sin(\Phi/2). \quad (7)$$

BS spectrometers as IN16 can also be used in a different operation mode, known as the fixed-elastic-window (FEW) technique. In this technique the monochromator is held fixed and the sample temperature is varied at a moderate rate. In this way one measures the elastic intensity as a function of the temperature, since the FEW technique only detects the fraction of neutrons with an energy exchange within the instrumental resolution. Hence, what is considered as elastic intensity depends on the resolution of the used spectrometer. For IN16, with a resolution function of HWHM $\approx 0.45 \mu\text{eV}$, the dynamics of scattering particles being slower than a characteristic time $\tau \approx 10 \text{ ns}$ are observed as elastic scattering. When increasing temperature, T , the fraction of particles slower than τ decreases, yielding a decrease of the elastic intensity. This decrease is exponential if dynamics in that time scale is purely vibrational, and it is given by the Q -dependent Debye-Waller factor $e^{-2W(Q)}$ [37–40], with $W(Q) = Q^2 \langle u^2 \rangle / 3$. In this expression $\langle u^2 \rangle$ is the mean-squared displacement per particle. For vibrational motions $\langle u^2 \rangle \propto T$. The presence of other dynamic processes is evidenced by deviations from exponential behavior, yielding a step-like decay of the elastic intensity (see Section VI).

The spectrometer D7 combines TOF methods with spin polarization analysis capabilities [44,45]. Among the different types of experiments which are possible

with D7, that of particular interest for the investigation of methyl group dynamics in polymers is the measurement of the coherent and incoherent contributions to the total scattered intensity (without energy analysis). These measurements are usually performed at low temperature to ensure that no significant intensity is lost due to the finite range of energy transfer covered by the instrument. By using a neutron incident wavelength of 4.8 \AA , the relevant accessible Q -range, $Q \lesssim 2.5 \text{ \AA}^{-1}$, corresponds to that covered in dynamic experiments with TOF and BS instruments.

In TOF instruments as IN5 or IN6, high values of vibrational frequencies are only accessible in neutron energy gain. Since the thermal statistical weight of high-energy vibrational excitations is negligible at low temperature, such excitations can only be detected by the former instruments at high temperature. This becomes a problem for the observation of methyl group librational peaks, which, due to anharmonicity effects, show a strongly damped intensity at high temperature [47–50]. This problem can be avoided by using an instrument which has access to vibrational frequencies in neutron energy loss, i.e., which is able to create the corresponding vibrational excitations in the sample even at very low temperature. An example of a TOF spectrometer that is optimized for vibrational spectroscopy is TOSCA [46], which allows one to measure neutron energy loss in a wide range of values, typically $1 \text{ meV} \lesssim \hbar\omega \lesssim 250 \text{ meV}$. TOSCA design is such that there is a unique value of Q for each value of the energy transfer, so all the detectors are summed up to obtain the vibrational spectrum. The arrangement of the spectrometer is such that the neutrons are detected at a fixed scattering angle $\Phi = 135^\circ$. In this situation Eq. (6) reduces approximately to the relation $Q^2 \propto \omega$ for low values of the neutron energy transfer ($\hbar\omega \lesssim 40 \text{ meV}$). Hence, TOSCA arrangement provides a nearly direct access to the generalized vibrational density of states (VDOS), $Z(\omega)$, given by [37–40]:

$$Z(\omega) = \frac{S(Q, \omega)\omega}{Q^2[n(\omega) + 1]}, \quad (8)$$

where $n(\omega) = [\exp(\hbar\omega/k_B T) - 1]^{-1}$ is the statistical Bose occupation factor. It must be stressed that the generalized VDOS $Z(\omega)$ is not proportional to the real VDOS, but a "deformed" function, where excitations are weighted by scattering cross-sections, molecular masses, and coordinates of the normal modes. Only

for a strictly monoatomic sample $Z(\omega)$ is proportional to the real VDOS. In the general case, though the experimental peaks will correspond to the real excitations, their amplitudes will be controlled by the mentioned factors, being larger for the modes involving motions of protium hydrogens.

C. Final experimental considerations

Instrumental resolution functions are usually determined from measurements on a vanadium sample, which provides solely elastic scattering. The same measurements can be used to calibrate detectors. In order to obtain the actual experimental scattering function $S(Q, \omega)$, raw data must be corrected for detector efficiency, sample container and absorption. Due to its small scattering cross-section, aluminium is the usual material for sample holders. Slab geometry is usually preferred. The typical area of the neutron beam is of $10 - 15 \text{ cm}^2$. The sample thickness is selected to provide a transmission of $90 - 95 \%$. For fully protonated polymers this condition is attained with sample thickness of $\sim 0.1 \text{ mm}$. High transmission allows one to neglect multiple scattering effects, provided that the very low Q -range is not considered in the data analysis. This is the case for methyl group dynamics, since the EISF at low Q is very close to unity (see Fig. 3), and correspondingly, the quasielastic intensity — which is weighted by $1 - A(Q)$, see Section III — is very weak and difficult to analyze.

III. METHYL GROUP DYNAMICS IN CRYSTALLINE SYSTEMS: THEORY AND SCATTERING FUNCTIONS

A. Rotational tunnelling

As mentioned in the Introduction, methyl group motion at very low temperature ($T \sim 1 \text{ K}$) can be modelled as that of a rigid rotor in an effective single-particle one-dimensional rotational potential $V(\phi)$. The corresponding Hamiltonian is given by [5–7]:

$$H_R = -B \frac{\partial^2}{\partial \phi^2} + V(\phi). \quad (9)$$

In this equation $B = \hbar^2/2I$ is the rotational constant of the rigid rotor, with I the moment of inertia of the

methyl group around its threefold symmetry axis. For a fully protonated methyl group $B = 0.655 \text{ meV}$. For a fully deuterated one, $B = 0.328 \text{ meV}$.

The rotational potential $V(\phi)$ must be invariant under $2n\pi/3$ rotations, with $n = \pm 1, \pm 2, \pm 3, \dots$, because its symmetry cannot be lower than that of the rigid rotor, and moreover, both symmetries cannot be incompatible. Hence, $V(\phi)$ can be expanded as a Fourier series of $3n$ -fold terms of amplitude V_{3n} :

$$V(\phi) = \sum_{n=1}^{\infty} \frac{V_{3n}}{2} [1 - \cos(3n\phi + \delta_{3n})], \quad (10)$$

where δ_{3n} are constant angular offsets. Indeed, it can be formally demonstrated that the rotor-lattice interaction can be expressed in this way provided that $V(\phi)$ is given by a sum of two-body additive potentials [51]. As mentioned in the Introduction, in a first approximation only the threefold term of the expansion is retained:

$$H_R = -\frac{\hbar^2}{2I} \frac{\partial^2}{\partial \phi^2} + \frac{V_3}{2} (1 - \cos 3\phi). \quad (11)$$

If higher-order terms are necessary to account for the experimental results, they often contribute just as small corrections to the main threefold term [5].

As mentioned in the Introduction, the coupling of the wavefunctions of the individual wells splits the librational levels. The resulting sub-levels are denoted as A and E , the latter consisting of the degenerate doublet (E_a, E_b). These labels correspond to the irreducible representations of the symmetry group C_3 of the Hamiltonian H_R . The eigenstate A remains unchanged under a rotation $2\pi/3$, while such an operation adds a phase $\pm 2\pi/3$ to the spatial part of the wave functions of E_a and E_b respectively. An eigenstate of H_R is characterized by two discrete quantum numbers, namely the librational, n , and symmetry, S , indexes: $|nS\rangle$. As shown in Fig. 1, the levels A and E alternate between consecutive librational levels.

At very low temperature, $T \sim 1 \text{ K}$, $k_B T \ll E_{0i}$ and the occupation probability of the excited librational states $i = 1, 2, 3, \dots$ is negligible. Hence, the rotor oscillates coherently between the three wells with an oscillation frequency equal to the tunnelling frequency ω_t . If the latter takes a value between the highest resolution available in BS spectrometers, $\hbar\omega_t \approx 0.3 \mu\text{eV}$, and the free rotor limit, $\hbar\omega_t = B$, it is detected as two

resolution-width inelastic peaks at $\omega = \pm\omega_t$ (see Fig. 4a).

The incoherent scattering functions for rotational tunnelling in different symmetries can be calculated by using symmetry adapted scattering operators [6]. Hence, the incoherent scattering operator

$$W = \sum_{j=1}^N (\mathbf{S} \cdot \mathbf{I}_j) \exp(-i\mathbf{Q} \cdot \mathbf{r}_j) \quad (12)$$

where \mathbf{r}_j , \mathbf{I}_j are the hydrogen positions and spins, and \mathbf{S} is the neutron spin, can be rewritten, for threefold symmetry, as:

$$W = W_A + W_{E_a} + W_{E_b}. \quad (13)$$

The eigenstates $|A\rangle$, $|E_a\rangle$ and $|E_b\rangle$ are unchanged by W_A , and are permuted cyclically by W_{E_a} , and anti-cyclically by W_{E_b} . Hence, the decomposition (13) allows for a straightforward calculation of the W -matrix elements between the different eigenstates [6]. After averaging over all the orientations of the scattering vector \mathbf{Q} , the following transition amplitudes are obtained:

- i) $f_{AE}(Q) = [1 - j_0(Qr)]/3$ for $A \leftrightarrow E$ (E_a, E_b) transitions. The corresponding contribution to the scattering function is $2f_{AE}(Q)\delta(\omega \pm \omega_t)$, since there are two inelastic transitions $\omega = +\omega_t$ and other two $\omega = -\omega_t$.
- ii) $f_{E_a E_b}(Q) = [1 - j_0(Qr)]/3$ for $E_a \leftrightarrow E_b$ transitions. These two elastic transitions contribute as $2f_{E_a E_b}(Q)\delta(\omega)$.
- iii) $f_{NSC}(Q) = [1 + 2j_0(Qr)]/3$ for transitions without symmetry change. These three elastic transitions contribute as $3f_{NSC}(Q)\delta(\omega)$.

In these expressions, $j_0(Qr) = \sin(Qr)/Qr$, with r the H-H distance in the methyl group, ($r = 1.78 \text{ \AA}$). After normalization to one-hydrogen scattering, the corresponding incoherent scattering function for methyl group tunnelling is [5-7]:

$$S_{\text{inc}}^{\text{MG}}(Q, \omega) = \frac{5 + 4j_0(Qr)}{9} \delta(\omega) + \frac{2[1 - j_0(Qr)]}{9} [\delta(\omega + \omega_t) + \delta(\omega - \omega_t)]. \quad (14)$$

The EISF, $A(Q) = [5 + 4j_0(Qr)]/9$, and $[1 - A(Q)]/2 = 2[1 - j_0(Qr)]/9$, which modulate respectively the elastic and inelastic contributions, are shown in Fig. 3.

B. Crossover from rotational tunnelling to classical hopping

The usual temperature dependence of neutron scattering spectra for methyl group dynamics in crystalline systems is illustrated in Fig. 4 for crystalline sodium acetate trihydrate [36]. At $T \sim 1 \text{ K}$ (Fig. 4a) the spectrum shows a central elastic peak and two inelastic peaks of resolution width, i.e., delta functions convoluted with the instrumental resolution. According to the picture exposed above, the inelastic peaks correspond to the two transitions $A \leftrightarrow E$ within the ground librational state. The elastic peak includes the ground state transitions $E_a \leftrightarrow E_b$ and the transitions without symmetry change. It also includes the elastic incoherent contribution from other atoms different from methyl group hydrogens, and the total coherent contribution (see below).

When increasing temperature [36,48,50,52-59], the inelastic peaks progressively broaden and shift to the elastic peak. At the same time, a quasielastic component appears around the elastic peak, and broadens with increasing temperature (Figs. 4b,c). Finally, in a narrow temperature interval ($\Delta T \sim 7 \text{ K}$), the quasielastic and inelastic components merge in a single quasielastic line (Fig. 4d). In the following the width of this interval will be neglected and represented as a unique temperature T_c , that will be denoted as the *crossover temperature*. Above T_c , a classical picture of thermally activated hopping over the rotational barrier is commonly accepted [6,37]. The observed single quasielastic line is well described by a Lorentzian function. The corresponding HWHM follows an Arrhenius-like temperature dependence:

$$\Gamma = \Gamma_\infty \exp(-E_A/k_B T). \quad (15)$$

where the classical activation energy E_A , as mentioned in the Introduction, is defined as the difference between the top of the barrier and the ground state (see Fig. 1). In the following E_A will be given in units of k_B . The preexponential factor Γ_∞ is temperature independent and typically takes values of $\sim 5 - 10 \text{ meV}$.

While rotational tunnelling and classical hopping are well established pictures respectively in the low and high temperature limits, no satisfactory theory for the crossover regime between both dynamic limits has won general acceptance [9-14,60-65]. Every model

for the crossover regime must give account for the following phenomenology observed in a large amount of experiments [36,48,50,52–59]:

i) Broadening of the quasielastic and inelastic crossover components are well described by Lorentzian functions of the same intensity. The relative intensities to the elastic peak are the same than in the purely rotational tunnelling regime, i.e., $2f_{AE}(Q)/3f_{NSC}(Q)$ for each of the inelastic lines and $2f_{E_aE_b}(Q)/3f_{NSC}(Q)$ for the quasielastic line. The temperature dependence of the Lorentzian HWHM follows Arrhenius-like behavior. The observed activation energy corresponds approximately to the first librational energy:

$$\Gamma_i = \gamma_i \exp(-E_{01}/k_B T). \quad (16)$$

$$\Gamma_q = \gamma_q \exp(-E_{01}/k_B T). \quad (17)$$

In these equations Γ_i and Γ_q are respectively the Lorentzian HWHM for the inelastic and quasielastic components. The preexponential factors γ_i and γ_q are temperature independent, and typically take values in the range 0.05-1 meV, much lower than the observed values for the classical Γ_∞ (see above). It is usually found that $\gamma_q < \gamma_i$, though both factors take values of the same order of magnitude (typically $\gamma_q/\gamma_i \sim 0.5$).

ii) Shift of the tunnelling peaks also follows Arrhenius-like behavior:

$$\hbar\Delta\omega_t = \gamma_s \exp(-E_S/k_B T), \quad (18)$$

where $\Delta\omega_t$ is the shift (in absolute value) of the tunnelling peak and γ_s a temperature independent preexponential factor, which takes values similar to γ_i and γ_q . The activation energy E_S is generally smaller than E_{01} though it takes a close value, typically $E_S/E_{01} \sim 0.7$. Fig. 5 shows all these features for crystalline sodium acetate trihydrate as a standard showcase [36].

All the theoretical models that aim to give account for these universal features state that its physical origin is the coupling of the methyl group to the lattice phonons, which progressively breaks the coherence of the wavefunction of the rotor, leading to incoherent tunnelling [9–14,51,60–84]. The standard approach,

and the only one that is able to give account quantitatively for the observed behavior, at least below T_c , is to describe the system rotor-lattice by a Hamiltonian:

$$H = H_R + H_B + H_C. \quad (19)$$

In this equation H_R is the rigid rotor Hamiltonian (9), H_B is a bath of harmonic oscillators [9,11–13,64,71–73,75–79,82,84]:

$$H_B = \sum_{k=1}^N \left(-\frac{\hbar^2}{2m_k} \frac{\partial^2}{\partial x_k^2} + \frac{1}{2} m_k \omega_k^2 x_k^2 \right), \quad (20)$$

and H_C is a coupling term between the rotor and the bath:

$$H_C = \sum_{k=1}^N g_k x_k \cos(3\phi + \delta_k). \quad (21)$$

In these equations x_k , m_k , ω_k , g_k and δ_k are respectively the displacements, masses and frequencies of the harmonic oscillators, the coupling constants and the angular offsets relative to the rotor.

The total Hamiltonian (19) retains the threefold symmetry of the interactions methyl group - environment. Hence, an argumentation on the basis of transitions between different symmetry states is still possible. The eigenvectors of the Hamiltonian (19) are characterized by a large set of quantum numbers. However, since H is, as H_R , unvariant under the symmetry group C_3 , the symmetry indexes A , E_a and E_b are still good quantum numbers for H , and the symmetry adapted formalism can still be used to calculate the scattering function. In the limit $N \rightarrow \infty$, H has a continuous number of eigenstates. Hence, transitions with symmetry change will take place not between two discrete eigenstates, but between two continuous sets of eigenstates. The delta functions for the low temperature limit [Eq. (14)], corresponding to transitions between two eigenstates characterized by a symmetry index, are now substituted by Lorentzians, corresponding to transitions between two large sets of eigenstates, each set characterized by a symmetry index, i.e.,

$$|\xi S\rangle \rightarrow |\xi' S'\rangle, \quad (22)$$

where S and S' are the initial and final symmetry states, and ξ and ξ' a large set of quantum numbers characterizing the initial and final state of the bath.

Within this picture, the inelastic Lorentzians involve transitions $A \leftrightarrow E$, while the quasilelastic Lorentzian involve transitions $E_a \leftrightarrow E_b$. Hence, Eqs. (16,17) can be rewritten as:

$$\Gamma_{AE} = \gamma_{AE} \exp(-E_{01}/k_B T) \quad (23)$$

$$\Gamma_{E_a E_b} = \gamma_{E_a E_b} \exp(-E_{01}/k_B T). \quad (24)$$

It can be demonstrated that elastic transitions without symmetry change do not lead to broadening [13], yielding an elastic line as in the low temperature limit. Taking all this arguments into account, the incoherent scattering function for the crossover regime is given by [48,77]:

$$S_{\text{inc}}^{\text{MG}}(Q, \omega) = \frac{1 + 2j_0(Qr)}{3} \delta(\omega) + \frac{2[1 - j_0(Qr)]}{9} \times \\ [L(\omega; \Gamma_{E_a E_b}) + L(\omega + (\omega_t - \Delta\omega_t); \Gamma_{AE}) + \\ L(\omega - (\omega_t - \Delta\omega_t); \Gamma_{AE})], \quad (25)$$

where $L(\omega - \nu; \eta)$ is a Lorentzian function of area unity, centered at $\omega = \nu$ and HWHM $= \eta$, i.e.:

$$L(\omega - \nu; \eta) = \frac{1}{\pi} \frac{\eta}{(\omega - \nu)^2 + \eta^2}. \quad (26)$$

It must be stressed that the functional form (25) is a direct consequence of the threefold symmetry of the Hamiltonian (19). It is the description of the temperature dependence of shift and broadening of the Lorentzian lines which depends on the particular model for the coupling of the rotor to the bath [Eqs. (20, 21)]. In the different models based on this approach, Eqs. (23, 24) are obtained as effective expressions from a sum over complicated functions containing Bose factors resonant on the librational frequencies, the density of states $\mathcal{Z}(\omega)$ and the coupling constants $\{g_k\}$:

$$\Gamma_{\xi\xi'} = \sum_{j=1}^N \mathcal{G}_{\xi\xi'}[\mathcal{Z}(E_{0j}), \{g_k\}, n(E_{0j})], \quad (27)$$

with $\xi\xi' = AE$ or $E_a E_b$, and $n(\omega)$ the Bose occupation factor. In practice, for the temperature range $T < T_c$, where the crossover regime is experimentally observed, one has $k_B T \ll E_{01}$. Hence, the sum (27) is dominated by the term in E_{01} and can be approximated as $\Gamma_{\xi\xi'} = \gamma_{\xi\xi'} \exp(-E_{01}/k_B T)$, in agreement with Eqs (23, 24).

For the case of the shift of the tunnelling frequency, the sum is done over all the phonon spectrum:

$$\hbar\Delta\omega_t = \int_0^\infty d\omega \mathcal{G}_s[\mathcal{Z}(\omega), \{g_k\}, n(\omega)]. \quad (28)$$

Again for $k_B T \ll E_{01}$ the integral can be approximated as an effective Arrhenius equation as (18). Since the integration is done over all the phonon spectrum, it is dominated by low-energy contributions, yielding an effective activation energy E_S smaller but close to E_{01} .

There is a strong controversy about the validity of the model given by Eqs. (19,20,21) for arbitrarily high temperatures. Some authors have claimed [64,77] that it is a valid picture even above T_c , the temperature above which spectra are well described by the classical hopping model. According to this statement, the observed classical-like Arrhenius behavior (15) is also obtained as an effective expression of the sum (27), where the highest order contributions would lead, at high temperature, to the observed apparent activation energy E_A , which is higher but close to the highest librational transition (see Fig 1).

C. Classical hopping

The incoherent scattering function above T_c can be derived in a classical hopping picture, disconnected from the low temperature quantum features above described. A master equation [6,37] is assumed for the classical probabilities (denoted as p_1, p_2, p_3) of finding the rotor in each of the three equilibrium positions $0, \pm 2\pi/3$:

$$\begin{aligned} \dot{p}_1 &= \frac{1}{\tau} \left[-p_1 + \frac{p_2}{2} + \frac{p_3}{2} \right] \\ \dot{p}_2 &= \frac{1}{\tau} \left[-p_2 + \frac{p_3}{2} + \frac{p_1}{2} \right] \\ \dot{p}_3 &= \frac{1}{\tau} \left[-p_3 + \frac{p_1}{2} + \frac{p_2}{2} \right]. \end{aligned} \quad (29)$$

The hopping time between two equilibrium positions is assumed to be negligible in comparison with the residence time, τ , between consecutive jumps. This assumption is confirmed (see e.g., [85–88]) by molecular dynamics simulations (MDS), which allow one to observe the motion of each individual methyl group in

the system. Fig. 6 shows computed angular positions for a methyl group hindered by a moderate barrier. As can be seen, sudden jumps occur between the three equilibrium positions, with long intervals between consecutive jumps. It is worth emphasizing that τ is an average value over all the time intervals between consecutive jumps *of a same methyl group*. The fact that the latters take different values is a consequence of the stochastic nature of the hopping process. For a crystalline system with a unique barrier, τ will be the same for all the individual methyl groups. For a disordered system, τ will be different for each individual methyl group, as will be discussed in Section IV.

After solving the master equation (29), averaging over all the orientations of \mathbf{Q} , and Fourier transforming to the frequency domain, the following expression is obtained [6,37]:

$$S_{\text{inc}}^{\text{MG}}(Q, \omega) = \frac{1 + 2j_0(Qr)}{3} \delta(\omega) + \frac{2[1 - j_0(Qr)]}{3} L(\omega; \Gamma), \quad (30)$$

where $\Gamma = 3\tau/2$ is just assumed to follow the classical Arrhenius-like behavior of Eq. (15). The EISF, $A(Q) = [1 + 2j_0(Qr)]/3$, and $1 - A(Q) = 2[1 - j_0(Qr)]/3$, which modulate respectively the elastic and quasielastic contributions, are shown in Fig. 3.

D. Additional remarks

It must be noted that, as required by a consistent description of the temperature dependence of the spectra, the scattering function (25) for the crossover regime is reduced to Eqs. (14) and (30) respectively in the low and high temperature limits. For very low temperature, shift and broadening in Eqs. (18,23,24) tend to zero, recovering Eq. (14). On the other hand, tunnelling is suppressed above the crossover temperature, i.e., $\Delta\omega_t = \omega_t$, and the three Lorentzians merge into a single line if $\Gamma_{AE} = \Gamma_{E_a E_b} = \Gamma$. Hence, Eq.(30) is recovered.

Finally, the total scattering function $S(Q, \omega)$ is obtained by adding the incoherent contribution of the other atoms, and the total coherent contribution. If, except for methyl group rotation and lattice vibrations, no other dynamics are present in the considered dynamic window, the former contributions are elastic, and $S(Q, \omega)$ is given by:

$$S(Q, \omega) = e^{-2W(Q)} [\sigma_{\text{coh}} S(Q) \delta(\omega) + (\sigma_{\text{inc}} - \sigma_{\text{inc}}^{\text{MG}}) \delta(\omega) + \sigma_{\text{inc}}^{\text{MG}} S_{\text{inc}}^{\text{MG}}(Q, \omega)], \quad (31)$$

with σ_{coh} and σ_{inc} the total coherent and incoherent cross-sections and $\sigma_{\text{inc}}^{\text{MG}}$ the incoherent cross-section of the three hydrogens of the methyl group. $\sigma_{\text{coh}} S(Q)$ is the coherent static intensity. As mentioned above, the Debye-Waller factor $e^{-2W(Q)}$ gives account for the intensity loss with increasing temperature due to vibrations. Since the Debye-Waller factor only enters as a scaling factor in the total scattering function, it can be removed in the analysis procedure of the experimental spectra. Finally, it must be stressed that the function $\tilde{S}(Q, \omega)$ to be compared with the experimental spectrum is given by the convolution of the total scattering function (31) with the instrumental resolution $R(Q, \omega)$:

$$\tilde{S}(Q, \omega) = \int S(Q, \omega) R(Q, \omega - \omega') d\omega' \quad (32)$$

In the following, comparison between experimental spectra and any of the theoretical scattering functions given above, will be understood as done after convolution of the latter with the instrumental resolution.

IV. METHYL GROUP DYNAMICS IN POLYMER SYSTEMS

A. Rotation Rate Distribution Model (RRDM)

In this Section we summarize the grounds of the RRDM. Though the RRDM was initially developed for polymer systems, it must be stressed that all its basic assumptions can, in principle, be also applied to non-polymeric disordered systems (see Section VII). In the framework of the RRDM [25,31–36,88–94], it is assumed that the only effect of the structural disorder on methyl group dynamics is to introduce a distribution of rotational barriers $g(V_3)$, originated from the different local environments felt by the individual methyl groups. A non-trivial assumption is that the distribution of distances between neighbouring methyl groups does not introduce significant coupling forces for the smallest distances, which, in particular, would modify the single-particle Hamiltonian (9) leading to a more complex energy level scheme [95–100].

According to this approach, the spectrum for the disordered system is simply obtained as a superposition of crystal-like spectra weighted by the distribution $g(V_3)$. Due to the normalization condition $\int g(V_3)dV_3 = 1$, the elastic terms in Eq. (31) are not affected by the introduction of the distribution. Hence, in the framework of the RRDM, $S(Q, \omega)$ for the glassy system is formally equal to Eq. (31). However, the introduction of $g(V_3)$ modifies the incoherent contribution for methyl group dynamics, which is given by:

$$S_{\text{inc}}^{\text{MG}}(Q, \omega) = \int_0^\infty g(V_3)S_{\text{inc}}^{\text{MG}}(Q, \omega, V_3)dV_3, \quad (33)$$

where each single crystal-like spectrum $S_{\text{inc}}^{\text{MG}}(Q, \omega, V_3)$ evolves with temperature according to the description given in Section III, summarized in Eqs. (14,15,18,23, 24,25,30). The different parameters controlling this evolution are therefore, *for each individual methyl group*:

i) the tunnelling frequency ω_t , first librational energy E_{01} , and classical activation energy E_A . These three quantities are direct functions of the potential barrier V_3 , and are obtained by calculating the eigenvalues of the Hamiltonian (9). Fig. 7 shows the corresponding results for the purely threefold case. Highly accurate numerical relations for the latter, in the range $V_3 < 3500$ K, are given by:

$$E_A(\text{K}) = 0.598V_3^{1.05}, \quad (34)$$

$$E_{01}(\text{meV}) = 0.470V_3^{0.548}, \quad (35)$$

$$\hbar\omega_t(\text{meV}) = 0.655 \left(1 + \frac{V_3}{2.67}\right)^{1.06} \exp[-(V_3/4)^{0.5}]. \quad (36)$$

In these equations V_3 is given in units of K.

ii) the preexponential factors Γ_∞ , γ_s , γ_{AE} and $\gamma_{E_a E_b}$ for the different Arrhenius-like equations (15,18,23,24).

iii) the crossover temperature $T_c(V_3)$, that determines which regime -crossover if $T < T_c(V_3)$ or classical hopping if $T > T_c(V_3)$ - governs the dynamics of a given methyl group of barrier height V_3 at moderate temperature T .

Glassy systems show broad distributions $g(V_3)$. For that reason, shift, broadening, and merging of the individual peaks with the quasielastic component, cannot be solved from the spectrum for the glass. On the other hand, it is expected that the temperature dependence of individual spectra is highly sensitive to the barrier height. In principle, methyl groups with high values of V_3 will reach the classical hopping regime at higher T_c than those with low values of V_3 . Moreover, there is a large set of parameters, namely the preexponential factors for shift and broadening, which depend on the unknown constants $\{g_k\}$ describing the coupling between the methyl group and the phonon bath [Eqs. (27,28)]. Such preexponential factors cannot be easily deduced for a glassy system, in contrast to the crystalline case [36,48,50,52–59], where shift and broadening of the single peaks can be directly observed and analyzed (see Figs. 4, 5). As mentioned above, the typical values of Γ_∞ observed in crystalline systems are in the same order of magnitude (a few meV), but γ_s , γ_{AE} and $\gamma_{E_a E_b}$ can take a wide range of values.

All these problems enormously complicate the analysis of the spectra in glassy systems. Next it is shown that many of the unknown present parameters, namely γ_{AE} , $\gamma_{E_a E_b}$ and γ_s , controlling the temperature dependence of the crystal-like spectrum for each individual methyl group, can be removed without the need of carrying out complex calculations, as it would be required by the introduction of a detailed model for the coupling of the methyl group to the glass vibrations. Instead, a functional relation between the crossover temperature and the barrier height, $T_c = T_c(V_3)$, is assumed [33–36]. It is found that a consistent description of the spectra in all the temperature range is possible in terms of only three parameters: the average and standard deviation of the barrier distribution $g(V_3)$, and the preexponential factor Γ_∞ for classical hopping.

In the approach introduced by the *general version* of the RRDM [33–36], the crossover temperature T_c is operationally defined as the temperature where the rate for coherent quantum tunnelling becomes equal to the rate for incoherent classical hopping, i.e., $\Gamma(T_c) = \hbar\omega_t$, or from Eq. (15):

$$kT_c = \frac{E_A}{\ln(\Gamma_\infty/\hbar\omega_t)}. \quad (37)$$

As mentioned above, the classical activation energy

E_A and the tunnelling frequency ω_t are direct functions of V_3 . It has been shown (see Refs. [25,35] for a detailed discussion) that Γ_∞ can be taken as a barrier-independent quantity in a good approximation. Therefore, T_c defined in this way depends only on the barrier height V_3 and the preexponential factor for classical hopping Γ_∞ . This latter material-dependent parameter can be interpreted as a measure of the strength of the coupling of the methyl groups to the glass vibrations. For a given methyl group of barrier V_3 , the larger Γ_∞ —i.e., the stronger the coupling—, the lower will be the T_c for the onset of classical hopping. Two technical approximations are introduced:

i) For each individual methyl group, the preexponential factors γ_{AE} and $\gamma_{E_a E_b}$ are taken as equal (in the following they will be denoted as γ_b). Therefore,

$$\Gamma_{AE} = \Gamma_{E_a E_b} = \gamma_b \exp(-E_{01}/k_B T). \quad (38)$$

ii) The activation energy E_S for the shift of the tunnelling lines is assumed to be equal to E_{01} :

$$\hbar \Delta \omega_t = \gamma_s \exp(-E_{01}/k_B T). \quad (39)$$

The general experimental evidence in crystalline systems for the values of γ_{AE} , $\gamma_{E_a E_b}$ and E_S (see above) supports the reliability of these two approximations. In addition, two constraints are imposed to Eqs. (38,39) at the crossover temperature:

i) The tunnelling frequency must be shifted to zero at the onset of the classical regime, $\Delta \omega_t(T_c) = \omega_t$, as required by the disappearance of quantum effects above T_c . Hence, from Eq. (39):

$$\gamma_s = \hbar \omega_t \exp(E_{01}/k T_c) \quad (40)$$

ii) Continuity condition for the HWHM of the Lorentzians at the merging point T_c , i.e., $\Gamma_{AE}(T_c) = \Gamma_{E_a E_b}(T_c) = \Gamma(T_c)$. Hence, from Eqs. (15,38):

$$\gamma_b = \Gamma_\infty \exp[(E_{01} - E_A)/k T_c]. \quad (41)$$

A straightforward consequence of Eqs. (37,40,41) is that $\gamma_s = \gamma_b$, which is also in agreement with the generally close values found for both quantities in crystalline systems.

All the quantities at the right sides of Eqs. (37,40,41) depend exclusively on V_3 and on the barrier-independent factor Γ_∞ . In this way, the preexponential factors for the crossover, γ_b and γ_s , can be determined unambiguously for each value of V_3 in the distribution $g(V_3)$. Hence, the temperature dependence of the spectra for the glass is modelled exclusively in terms of Γ_∞ and $g(V_3)$. Two-parameter (average barrier and standard deviation) simple distributions are used, as Gaussian [25,31–34,36,88–93] functions. In a few cases [35,94] two-parameter Gamma functions are more adequate. In this way, the RRDM only introduces three independent parameters for the analysis of experimental spectra in all the temperature range.

In the limit of low and high temperature, all the individual methyl groups will perform respectively rotational tunnelling or classical hopping, and the corresponding crystal-like contributions to the spectrum of the glass [Eq. (33)] will be governed respectively by Eq. (14) for tunnelling and by Eqs. (15,30) for hopping. These limits are referred to as the *tunnelling* and *hopping* limits of the RRDM. At intermediate temperature the functional relation between T_c and V_3 introduced in Eq. (37) allows one to select the corresponding dynamic regime for each individual methyl group —i.e., crossover, governed by Eqs. (25,38,39,40,41), or classical hopping, governed by Eqs. (15,30).

In a first approximation, a Gaussian distribution of purely threefold rotational barriers is assumed:

$$g(V_3) = \frac{1}{\sqrt{2\pi}\sigma_V} \exp\left[-\frac{(V_3 - \langle V_3 \rangle)^2}{2\sigma_V^2}\right], \quad (42)$$

with $\langle V_3 \rangle$ the average barrier and σ_V the standard deviation of the distribution. See Fig. 8a for $\langle V_3 \rangle = 800$ K, $\sigma_V = 250$ K, as an example of parameters for which tunnelling and hopping features are observable by neutron scattering (see below).

The functional relations —e.g., Eqs. (34,35,36)— between E_A , E_{0i} , $\hbar \omega_t$, and V_3 , allow for a straightforward transformation between $g(V_3)$ and the corresponding distributions of activation energies for classical hopping, $f(E_A)$, rotational tunnelling frequencies, $h(\hbar \omega_t)$, and librational energies, $F(E_{0i})$:

$$\begin{aligned} g(V_3) dV_3 &= f(E_A) dE_A = \\ F(E_{0i}) dE_{0i} &= -h(\hbar \omega_t) d(\hbar \omega_t). \end{aligned} \quad (43)$$

In a good approximation, the classical activation energy E_A depends linearly on V_3 (see Fig. 7c).

Hence, the distribution $f(E_A)$ is also Gaussian (see Fig. 8b), with average energy $\langle E_A \rangle$ and standard deviation σ_E . As mentioned above, the preexponential factor for classical hopping Γ_∞ is assumed to be barrier-independent. This approximation allows one, according to Eq (15), to transform the Gaussian distribution $f(E_A)$ into a log-Gaussian distribution of Lorentzian HWHM for classical hopping:

$$H(\log \Gamma) = \frac{1}{\sqrt{2\pi}\sigma} \exp \left[-\frac{(\log \Gamma - \log \Gamma_0)^2}{2\sigma^2} \right], \quad (44)$$

where

$$\Gamma_0 = \Gamma_\infty \exp(-\langle E_A \rangle / k_B T) \quad (45)$$

is the corresponding Lorentzian HWHM for the average activation energy, and

$$\sigma = \sigma_E \log(e) / k_B T \quad (46)$$

is the standard deviation for $H(\log \Gamma)$. Fig. 9 shows the temperature dependence of this distribution for the above parameters $\langle V_3 \rangle = 800$ K, $\sigma_V = 250$ K, and for a typical value of $\Gamma_\infty = 6$ meV. As can be seen, at high temperature the major part of the distribution is accessible in the energy window of neutron scattering spectrometers.

The parameters Γ_0 and σ at a given high temperature can be obtained from a fitting procedure of the experimental methyl group incoherent contribution $S_{\text{inc}}^{\text{MG}}(Q, \omega)$ to the classical limit of Eq. (33). From the transformation $g(V_3)dV_3 = -H(\log \Gamma)d(\log \Gamma)$, and from the incoherent scattering function (30) for a single barrier, Eq. (33) can be rewritten in the classical limit as:

$$S_{\text{inc}}^{\text{MG}}(Q, \omega) = \frac{1 + 2j_0(Qr)}{3} + \frac{2[1 - j_0(Qr)]}{3} \int_{-\infty}^{\infty} H(\log \Gamma) L(\omega; \Gamma) d(\log \Gamma). \quad (47)$$

The set of values $\Gamma_0(T)$ and $\sigma(T)$ obtained for the different temperatures is fitted to Eqs. (45,46) in order to obtain Γ_∞ , $\langle E_A \rangle$ and σ_E . Finally, the knowledge of these two latter quantities allows, by transformation, to determine $\langle V_3 \rangle$ and σ_V , i.e., the parameters of the barrier distribution $g(V_3)$. The latter, as obtained from the analysis of classical high temperature spectra, can next be transformed into the distribution of tunnelling frequencies $h(\hbar\omega_t)$ and librational

energies $F(E_{01})$ (see Figs. 8c, 8d). The consistency of the RRDM requires that these two latter distributions derived in this way, also reproduce, respectively, the corresponding experimental tunnelling and librational spectra.

Due to the approximate exponential dependence of $\hbar\omega_t$ on V_3 (see Eq. (36) or Fig. 7a), $h(\hbar\omega_t)$ takes an extremely asymmetric shape (see Fig. 8d) with the maximum shifted to low frequencies. From the incoherent scattering function for a single barrier (14), the tunnelling limit of Eq. (33) is given by:

$$S_{\text{inc}}^{\text{MG}}(Q, \omega) = \frac{5 + 4j_0(Qr)}{9} \delta(\omega) + \frac{2[1 - j_0(Qr)]}{9} [h(\omega_t) + h(-\omega_t)]. \quad (48)$$

For sufficiently high average barriers $\langle V_3 \rangle$ or broad distributions $g(V_3)$, the maximum of $h(\pm\hbar\omega_t)$ is placed beneath the instrumental resolution (see Fig. 8d). Hence, the tunnelling spectrum shows an apparently quasielastic contribution, which could be misinterpreted as a signature of hopping events at very low temperature. However, its actually *inelastic* origin finds a natural explanation, within the framework of the RRDM, in terms of a distribution of rotational tunnelling lines.

Once the tunnelling and hopping limits of the RRDM are able to give account, with the same set of parameters $\langle V_3 \rangle$, σ_V and Γ_∞ , respectively for the experimental spectra at very low and high temperature, the consistency of the general version of the RRDM is tested, with such parameters, at intermediate temperature. It must be noted that this step does not involve any further fitting procedure. Instead, experimental spectra are directly compared with the theoretical ones, which are constructed according to the procedure exposed above for the general version of the RRDM, and by making use of the operational definition of the crossover temperature, Eq. (37), in order to select the dynamic regime (crossover or classical) for each individual methyl group.

Eq. (37) also introduces a distribution of crossover temperatures, $G(T_c)$. Fig. 10 shows the latter, for the same parameters, $\langle V_3 \rangle = 800$ K, $\sigma_V = 250$ K and $\Gamma_\infty = 6$ meV, of Figs. 8 and 9. As temperature T increases, the fraction of methyl groups that reach the classical hopping regime, i.e., the area of $G(T_c)$ for $T_c < T$, will also increase and will be negligible above

some high temperature, where quantum effects will be unsolvable from the dominating hopping dynamics. In such conditions, the system will be well described by the classical limit of the RRDM.

B. Other approaches

An alternative approach to the classical limit of the RRDM, also based on the idea of an underlying distribution of rotational barriers, has been introduced by Arrighi *et al.* [23,24] for analyzing methyl group dynamics in the high temperature hopping regime. By Fourier transforming into the time domain, the intermediate incoherent scattering function for methyl group classical hopping is given by:

$$I_{\text{inc}}^{\text{MG}}(Q, t) = \frac{1 + 2j_0(Qr)}{3} + \frac{2[1 - j_0(Qr)]}{3} \mathcal{F}(t). \quad (49)$$

Obviously for a crystalline system $F(t) = \exp(-t/\tau)$, with τ the *single* residence time for hopping.

For a disordered system, the corresponding function $\mathcal{F}(t)$ in the framework of the RRDM is a log-Gaussian distribution of time exponential functions:

$$\mathcal{F}(t) = \int_{-\infty}^{\infty} H(\log \tau) \exp(-t/\tau) d(\log \tau), \quad (50)$$

as trivially obtained by Fourier transformation of Eq. (47). In the approach introduced by Arrighi *et al.*, no functional form is assumed for the distribution $H(\log \tau)$. On the contrary, $\mathcal{F}(t)$ is effectively represented by a stretched exponential, or Kohlraush-Williams-Watts (KWW) function, $\exp[-(t/\tau_0)^\beta]$, with τ_0 a characteristic rotational relaxation time. The stretching exponent β takes values between 0 and 1.

A KWW function can be effectively represented as a log-distribution of time exponential functions:

$$\exp[-(t/\tau_0)^\beta] = \int_{-\infty}^{\infty} K(\log \tau) \exp(-t/\tau) d(\log \tau). \quad (51)$$

The distribution function $K(\log \tau)$, which can be obtained by inverse Laplace transformation methods [101], is asymmetric. Therefore it is clear that the KWW function cannot be equivalent to the RRDM distribution $\mathcal{F}(t)$ if a log-Gaussian form is selected for $H(\log \tau)$ [89], (note that for the same reason $\tau_0 \neq \tau$). This fact is illustrated in Fig. 11 for typical values $\tau = 0.1$ ns and $\sigma = 1$.

Both pictures (KWW and RRDM) achieved descriptions of similar quality for experimental spectra in a limited energy window, i.e., by using a single spectrometer. The corresponding times τ and τ_0 followed Arrhenius behavior with close values of the respective activation energies [23,24,89]. However, an analysis in a wide dynamic range [89], by combining several spectrometers, showed that, while an excellent agreement of the experimental $\mathcal{F}(t)$ with the RRDM function (50) was obtained in all the time interval, a simultaneous fit to a KWW function was not satisfactory. Moreover, independent fits in different experimental windows provided incompatible values of τ_0 and β . This result is illustrated in Fig. 12 for the same function $\mathcal{F}(t)$ of Fig. 11, now analyzed in different narrow dynamic windows.

Another disadvantage of using a KWW functional form for $\mathcal{F}(t)$ is that, in contrast to the unified picture introduced by the RRDM, it does not provide a direct physical connection between the classical and quantum features observed respectively at high and low temperature. It is worthy of remark that MDS support, by following separately the behavior of each individual methyl group in the system, the general validity of the Gaussian approach for the distribution of rotational barriers [85,86,88,102].

V. APPLICATION OF THE RRDM TO A SHOWCASE: POLY(VINYL ACETATE)

PVAc was the first polymer—and indeed the first highly disordered system—where a complete investigation by neutron scattering was carried out on all the features of methyl group rotation (tunnelling, crossover, hopping and librations). It was also the first system where a fully consistent description of the experimental results was achieved in terms of the RRDM [31,33,89]. Figs. 13, 14 show respectively for a BS and a TOF spectrometer, experimental spectra (circles) for PVAc, at several temperatures in the tunnelling ($T = 2$ K), crossover ($T = 20$ and 30 K) and classical hopping ($T = 70, 120, 160$ and 200 K) regimes. All these temperatures are far below the glass transition temperature ($T_g \approx 315$ K), where motions different from methyl group rotation just contribute as vibrational dynamics via the Debye-Waller factor.

An excellent agreement with the RRDM is observed in all the temperature range (solid lines). As in the

usual analysis procedure, high temperature data of PVAc were first analyzed in terms of the classical RRDM [89]. Fig. 15 shows the temperature dependence of the parameters $\log \Gamma_0$ and σ of the distribution $H(\log \Gamma)$ (taken as Gaussian) obtained from the analysis in terms of the hopping limit of the RRDM. The use of several spectrometers with different energy resolutions and dynamic ranges reduced the uncertainties of the so determined parameters. The observed deviations below $T \approx 70$ K from the linear behavior predicted by Eqs. (45,46) show the relevance of quantum effects at low temperatures. The fact that the magnitude of such deviations depend on the experimental dynamic window evidences the importance of using several spectrometers in order to avoid, below some temperature, an analysis biased by the used instrumental resolution. The results of the fits for $T > 70$ K to Eqs. (45,46) provide a preexponential factor $\Gamma_\infty = 9.1$ meV, an average classical activation energy $\langle E_A \rangle = 450$ K, and a standard deviation $\sigma_E = 250$ K. Transformation to $g(V_3)$ yields $\langle V_3 \rangle = 534$ K and $\sigma_V = 274$ K. The dashed lines in Fig. 15, corresponding to $\Gamma = \Gamma_\infty \exp[-(\langle E_A \rangle \pm \sigma_E)/k_B T]$, have been introduced in order to stress the presence of a wide distribution of hopping times, which progressively spreads over several orders of magnitude as temperature decreases.

The corresponding distribution of tunnelling frequencies $h(\hbar\omega_t)$ is obtained by transformation of the barrier distribution $g(V_3)$ independently derived from the high temperature classical analysis. Once $h(\hbar\omega_t)$ is known, the theoretical $S_{\text{inc}}^{\text{MG}}(Q, \omega)$ is constructed according to Eq. (48). An excellent agreement between the tunnelling limit of the RRDM and the experimental spectrum at 2 K is obtained (Fig. 13). The maximum of $h(\hbar\omega_t)$ is at $\hbar\omega_t \approx 0.03$ μeV [31], i.e., well beneath the instrumental resolution, leading to the apparently quasielastic observed intensity .

For the case of the librational distributions, a direct comparison with experimental results is complicated, since librational energies are strongly superposed with the phonon spectrum. This is particularly problematic in PVAc, which cannot be selectively deuterated in order to attenuate the intensity scattered by nuclei different from methyl group protons. Fig. 16 shows a comparison of the generalized VDOS of PVAc with the distribution of librational energies $F(E_{01})$ obtained by transformation of $g(V_3)$. A reasonable agreement be-

tween the maximum of the experimental peak and the maximum of $F(E_{01})$ is achieved, supporting the validity of the previously obtained distribution $g(V_3)$ and the consistency of the RRDM picture. It must be stressed that, since the generalized VDOS is not the real density of states (see Section II), a rigorous comparison between the widths of the experimental librational peaks and the theoretical librational distributions cannot be made.

Once it has been checked that the distribution of potential barriers $g(V_3)$ can give account, by transformation to the other distributions in Eqs. (43, 44), for the spectra in the tunnelling and hopping dynamic limits, as well as for the librational peak observed in the generalized VDOS, the consistency of the general RRDM is confirmed by also reproducing the experimental spectra at intermediate temperatures (Fig. 13 for $T = 20$ and 30 K). An excellent agreement is again achieved. A more detailed comparison between experiment and theory can be obtained by investigating the temperature dependence of the integrated intensities in different inelastic windows, as shown in Fig. 17. Since Eq. (48) is temperature-independent, and the Debye-Waller factor is a decreasing function of T , the initial increase of the integrated intensities when heating the system makes clear that the tunnelling limit of the RRDM is not applicable for $T \gtrsim 2$ K. It must be stressed that the observed double-peak structure is not an experimental artifact. Indeed, it can also be observed in a crystalline system when the inelastic window is properly selected, e.g., at lower energy but close to the single tunnelling line. As mentioned in Section III, when increasing temperature the tunnelling line broadens and shifts to lower energies until it merges, when reaching the hopping regime, into a single quasielastic line. As a consequence, the intensity measured in the selected inelastic window will pass through a first maximum. A second maximum will be observed at higher temperature when broadening of the quasielastic line reaches the selected inelastic window. In glassy PVAc, due to the broad distribution of tunnelling frequencies in comparison with the energy window accessible by the spectrometer, the double-peak structure is observed at any inelastic window.

As shown in Fig. 17, the double-peak structure is nicely reproduced by the theoretical curves (solid lines) obtained by integration of the RRDM scattering

function in the corresponding inelastic windows. The theoretical curves quantitatively reproduce the experimental intensities in all the temperature range. It must be noted that the formers have been modulated by a Debye-Waller factor $e^{-2Q^2\langle u^2 \rangle/3}$, with $\langle u^2 \rangle = \theta T$ and $\theta = 3 \times 10^{-4} \text{ \AA}^2\text{K}^{-1}$ [31]. The theoretical curves corresponding to the classical hopping limit of the RRDM (dashed lines) have been extrapolated to very low temperature in order to stress the relevance of quantum effects below $T \approx 70 \text{ K}$, as was pointed out above.

VI. SUMMARY OF EXPERIMENTAL RESULTS BY NEUTRON SCATTERING ON POLYMERS

A. Classical hopping

From early 80's, neutron scattering has been widely used to investigate methyl group dynamics in the quasielastic energy range $|\hbar\omega| \lesssim 2 \text{ meV}$, or by using the FEW technique (see Section II). A huge collection of data has been obtained for several polymer systems, including standard materials as PVAc [89,103], PMMA [20,22–24,34,91,104], poly(propylene oxide) (PPO) [105], poly(vinyl methyl ether) (PVME) [23,25,27,106], polyisoprene (PI) [26,92], neat poly(dimethyl siloxane) (PDMS) [93,107–109], and filled with silica nanoparticles [110], head-to-tail [88,90], and head-to-head (hh) [111] polypropylene (PP), poly(ethylene propylene) (PEP) [111], and poly(methyl phenyl siloxane) (PMPS) confined in silica based nanoporous glasses [112], polymer blends as solution chlorinated polyethylene (SCPE)/PMMA [22,113], polystyrene (PS)/PVME [114,115], hh-PP/PEP [111], or poly(ethylene oxide) (PEO)/PMMA [116,117], thin film photoresist polymers [118], and other polymer based compounds as polymer electrolytes [119–121], proteins [122], liquid crystalline polyesters and polyethers [123,124] or propylene glycol oligomers in the bulk state [125] and confined in clay [126,127]. Very recently, Russina *et al.* have investigated methyl group classical hopping in a neat, and doped with an inorganic salt, PEO-PPO random copolymer [128]. Differently from the usual FEW technique, data have been acquired and analyzed in an *inelastic* fixed energy window centered at $\hbar\omega \approx -15\mu\text{eV}$ with BS resolution.

A simple way to investigate the temperature dependence of methyl group rotation is by following the temperature evolution of the FEW intensity, $I_{FEW}(Q, T)$ (see Section II). If the corresponding energy window for data acquisition is $-\Lambda_{el} \leq \hbar\omega \leq \Lambda_{el}$, then integration of Eq. (47), together with the additional elastic contributions (see Section III), provides the RRDM function for the FEW intensity:

$$I_{FEW}(Q, T) = e^{-2W(Q, T)} [\sigma_{\text{coh}} S(Q) + \sigma_{\text{inc}} - \sigma_{\text{inc}}^{\text{MG}} + \sigma_{\text{inc}}^{\text{MG}} I_{FEW}^{\text{MG}}(inc)(Q, T)], \quad (52)$$

where the incoherent contribution for methyl group classical hopping is given by [93]:

$$I_{FEW}^{\text{MG}}(inc)(Q, T) = \frac{1 + 2j_0(Qr)}{3} + \frac{2[1 - j_0(Qr)]}{3} \times \int_{-\infty}^{\infty} H(\log \Gamma) \frac{2}{\pi} \text{arctg} \left(\frac{\Lambda_{el}}{\Gamma} \right) d(\log \Gamma). \quad (53)$$

If temperature is sufficiently low so that most of the methyl groups rotate with a hopping rate $\Gamma \ll \Lambda_{el}$, the limit $(2/\pi)\text{arctg}(\Lambda_{el}/\Gamma) \rightarrow 1$ is fulfilled and $I_{FEW}^{\text{MG}}(inc)(Q, T) = 1$. In such conditions the temperature dependence of the FEW intensity is just controlled by the Debye-Waller factor, $I_{FEW}(Q, T) = e^{-2W(Q, T)} [\sigma_{\text{coh}} S(Q) + \sigma_{\text{inc}}]$. It must be reminded that below some temperature the classical hopping picture is not valid, and quantum effects dominate methyl group dynamics. However, from integration of Eqs. (48) and (25,33) in the FEW window, the latter result can be extrapolated to very low temperature if, for most of the methyl groups, Γ_{AE} , $\Gamma_{E_a E_b}$ and ω_t are all smaller than Λ_{el} .

FEW data for several polymers [26,90,93], obtained by means of high resolution BS spectrometers, are shown in Fig. 18. Intensities are normalized to their values at $T \rightarrow 0$. The onset of methyl group dynamics with time scales shorter than that corresponding to the instrumental resolution ($\sim 5 \text{ ns}$ for the used spectrometers) manifests as a step-like decrease of the normalized intensity, which, above some temperature, deviates from the exponential (linear in the logarithmic scale of Fig. 18) decrease corresponding to the Debye-Waller factor, i.e., to pure vibrational dynamics. The second step at the very high temperature range corresponds to the onset of much slower processes such as secondary relaxations or motions involved in the glass transition process.

The FEW technique requires much less acquisition time than QENS measurements, but obviously quasielastic spectra are preferred for an accurate determination of the parameters of the distribution of hopping rates. Though for moderate average barriers, analysis of FEW data have provided reliable results [90], this procedure is not recommended when the average rotational barrier is very high ($V_3 \gtrsim 2000$ K), since in such cases the two step-like decays of the FEW intensity overlap. Such a case is illustrated for polysulfone (PSF) in Figure 18.

First quasielastic investigations on methyl group classical rotation in polymers were analyzed in terms of the usual approach for molecular crystals, i.e., by using a single Lorentzian function (single hopping rate) to model the quasielastic component. As mentioned in the Introduction, such a procedure fails when applied to polymers (and in general to highly disordered systems), providing inconsistent and unphysical results. In polymeric materials, and in general in disordered systems [35,36], the effect of structural disorder has to be taken into account to describe properly methyl group dynamics. In the framework of the RRDM, it is assumed that the only effect of the structural disorder on methyl group dynamics is to introduce a distribution of rotational barriers $g(V_3)$, originating from the different local environments felt by the individual methyl groups. The initial version of the RRDM—the hopping limit— was introduced for analyzing quasielastic data from PVME [25]. Nearly at the same time, a very close approach based in a Gaussian distribution of activation energies was proposed by Frick and Fetters [26] to describe the temperature dependence of FEW data from PI. As mentioned in Section IV, an alternative approach [23,24], first introduced to analyze time-domain data of PMMA and PVME, assumed a KWW stretched exponential function for the intermediate scattering function $I(Q, t)$. Although this procedure was able to describe spectra obtained in a single spectrometer, it failed to properly account for data collected in a wide dynamic range by using several instruments [89].

Classical hopping between three equivalent positions was assumed in all these approaches. It must be noted that classical hopping is just driven by the activation energy E_A , and that a purely threefold barrier and another one distorted by a small sixfold contribution, $V_6(1 - \cos(6\phi + \delta))/2$, can provide the same E_A

with an appropriate selection of the parameters V_3 , V_6 and δ . Hence, an analysis of high temperature classical spectra provides a first approach to the functional form of the rotational potential, but an unambiguous determination of the latter is only possible by means of a complete analysis of hopping, tunnelling and librational spectra. For most of the polymers or molecular glasses for which at least two of these three features have been investigated, it has been found that a distribution of purely threefold barriers provides a good description of experimental spectra. As shown below, small but significant corrections to the threefold term have instead to be considered in order to consistently reproduce the different features of the ester-methyl group dynamics in PMMA.

Recent QENS investigations in PDMS [93], PVAc [103] and in the blends hh-PP/PEP [111], and PEO/PMMA [116] have tackled the problem of methyl group classical hopping in the very high temperature range where secondary relaxations or motions involved in the glass transition process enter the dynamic window of neutron scattering. In that situation the time scales of such processes and methyl group hopping superpose. A consistent description has been achieved by assuming that the mentioned motions and methyl group rotation are statistically independent. This approach was first introduced in an investigation, by means of molecular dynamics simulations, on methyl groups dynamics in PI above the glass transition temperature [129]. Within this approach, the RRDM picture is maintained for methyl group rotation and the total scattering function is just obtained as a convolution of the RRDM scattering function (47) and that corresponding to the other relaxational modes [129]. A unified description is achieved with the same values—or small variations— of the RRDM parameters derived at lower temperatures, where the dynamic contribution of the polymer matrix just enters in the vibrational Debye-Waller factor. This result evidences that the barrier distribution for methyl group rotation in polymers is not substantially changed by the structural rearrangements produced when approaching the glass transition [93,129].

B. Rotational tunnelling and crossover to hopping

As mentioned in the Introduction, the existence of quantum rotational tunnelling for methyl group dynamics in polymer systems was expected for a long time but it was not directly observed by neutron scattering until late 90's [31,32]. In contrast to crystalline systems where, due to the unique value of the rotational barrier, resolution-width tunnelling lines are observed at very low temperature, in amorphous systems, a distribution of rotational barriers, and therefore of tunnelling frequencies, is expected. Some examples are misoriented methyl groups in crystalline lattices [130] or absorbed in water clathrates [131] or crystalline zeolites [132], and other small molecular rotors in chemically or geometrically disordered environments as non-stoichiometric metal hexaammines [133], ammonia in metal alkali fullerenes [134], diluted solutions of methane in noble gases [135–137], or of ammonium in metal alkali halides [138,139]. In these systems, disorder effects provide narrow distributions of rotational barriers and of the corresponding tunnelling frequencies, which just manifest as weak broadening of the tunnelling peaks in neutron scattering spectra. However, in the case of methyl groups in polymers [31,32,34], molecular glasses [35,36], or close to pore walls in mesoporous silicates [94,140–142], disorder leads to broad distributions of tunnelling frequencies. Due to the typical values of the rotational barriers in the latter systems, specially in polymers, most of the expected distribution of tunnelling lines corresponds to energies below $\sim 1 \mu\text{eV}$, i.e., beyond the dynamic limit explored by BS spectrometers. This fact prevented for a long time the observation of tunnelling features in low temperature spectra.

PVAc is the polymer having the lowest energy barrier for methyl group rotation reported so far, and the most suitable one for the direct observation of rotational tunnelling transitions by means of neutron scattering [31,33]. An analogous investigation has been carried out on rotational tunnelling of the ester-methyl group of PMMA [32,34]. Though having a higher barrier, PMMA has the advantage of being selectively deuteratable, in contrast to PVAc. In this way, the observed scattered intensity excess for PMMA-d5 (i.e., with partial deuteration of the α -methyl group and the main-chain hydrogens) over the elastic line at very low temperature can be unambiguously assigned to the

ester-methyl group dynamics.

A further support of the interpretation of the apparently quasielastic low-temperature intensity as the result of a distribution of rotational tunnelling lines is provided by exploiting the well-known isotope effect. Hence, deuteration of the methyl group yields a rotational constant B twice smaller than for the protonated methyl group. The corresponding tunnelling frequency is reduced by several orders of magnitude (dashed line in Fig. 7a), and consequently, the corresponding distribution $h(\hbar\omega_t)$ is strongly shifted to lower frequencies (see Fig.19 for the ester-methyl group of PMMA). This effect predicts a strong suppression of the scattered intensity excess in the experimental spectrum, as it is indeed observed [32] in a fully deuterated sample (d8) of PMMA at the same temperature (see Fig. 20). For a proper comparison between the ester-methyl group dynamics in the d5- and d8-samples, the elastic contributions, corresponding to the total coherent cross-section and to the incoherent cross-section of the other nuclei, are subtracted from the spectra. This procedure introduces large uncertainties in the so obtained spectrum for the d8-sample, due to the large relative weight of such elastic contributions. However, the suppression in the d8-sample of the apparently quasielastic intensity is evident, and consistent with the result predicted on the basis of the RRDM parameters derived for the d5-sample [32].

Except for PVAc and for the ester-methyl group of PMMA, for the rest of the polymers investigated so far, the large values of the average barriers, $\langle V_3 \rangle \gtrsim 1000 \text{ K}$, determined from the analysis of high temperature hopping data and/or of librational levels, prevent the observation of clear rotational tunnelling features at very low temperature. This situation is illustrated in Fig. 21 by a comparison between the expected distributions of tunnelling frequencies for several polymers. As can be seen, within the neutron scattering window, $h(\hbar\omega_t)$ for PVME and PI is orders of magnitude smaller than for PVAc and for the ester-methyl group of PMMA. Convolution of $h(\hbar\omega_t)$ with the instrumental resolution provides a scattering intensity excess unsolvable from the latter within the experimental noise, as indeed is experimentally confirmed. An analysis of high temperature data for PDMS in terms of the hopping limit of the RRDM [93] provided a distribution of classical activation energies $f(E_A)$,

which, by transformation, would yield a distribution of tunnelling frequencies clearly observable by means of high-resolution BS spectrometers. However, the measured intensity at $T = 2$ K [143] is hardly distinguishable from the instrumental resolution, as can be seen in Fig. 22. Moreover, the RRDM parameters given in Ref. [93] provide, by transformation, a theoretical librational maximum around ≈ 17 meV, far from the experimental value of 21.2 meV (see Fig. 23a). On the contrary, the RRDM parameters in Ref. [89] reproduce the librational peak and are compatible with the experimental spectrum at $T = 2$ K (see Fig. 22). The reason for the mentioned incompatibilities with parameters in Ref. [93] remains to be understood.

Despite of the existence of very few polymer systems where methyl group rotational tunnelling can be observed by neutron scattering, successful investigations have been carried out in two molecular glasses —toluene [35] and sodium acetate trihydrate [36]— supporting the validity of the RRDM picture for rotational tunnelling.

As mentioned in Section IV, at the crossover intermediate temperature regime (typically $20 \text{ K} \lesssim T \lesssim 100 \text{ K}$) quantum effects are relevant for methyl group rotation, and quasielastic spectra cannot be reproduced in terms of the classical limit of the RRDM. However, the fact that spectra do not evolve with temperature according to the simple expectation for vibrational dynamics (see Section V) also evidences that the tunnelling limit of the RRDM cannot either be applied, and making use of the general version of the model is necessary. The crossover regime has been investigated in detail in the only two polymers (PVAc [33] and PMMA [34]) where the distribution of rotational tunnelling lines can be (partially) explored by neutron scattering. The success of the general version of the RRDM for reproducing all the temperature evolution of the spectra for both polymers has been extended to the glassy states of toluene [35] and sodium acetate trihydrate [36].

C. Librational levels

First neutron scattering experiments on methyl group dynamics were focused on the determination of the librational levels. Since early 70's INS investigations on methyl group librations have been per-

formed in a huge collection of polymeric materials as PPO [16], PP [144,145], PMMA [16,17,20,34], poly(α -methylstyrene) (P α MS) [17], PVAc [146], PDMS [146], PI [26,147], PIB [145,147,148], bisphenol-A based engineering thermoplastics as PSF, polycarbonate (PC) and phenoxy (PH) [149], and layered polytypes of hexatriacotane [150].

Figs. 16, 23, 24 and 25 show some examples of the experimental generalized VDOS for PVAc [146], PDMS [146], PMMA (ester-methyl group) [34], PI [26] and PSF [149], compared with the theoretical librational distributions $F(E_{01})$ obtained within the RRDM approach. For moderate and low energy barriers ($V_3 \lesssim 500 \text{ K}$), the lowest librational transitions occur in the same energy range (5 – 15 meV) where a broad shoulder in the generalized VDOS is observed for any disordered system [151]. This strong superposition complicates the identification and analysis of the corresponding librational peaks, as in the case of PVAc [146] (Fig. 16). On the contrary, for moderate and high rotational barriers ($V_3 \gtrsim 1000 \text{ K}$) as in PDMS, PI or PSF, librational peaks are well resolved from the generalized VDOS.

In order to solve methyl group librations, it is useful to carry out and compare INS measurements in samples with both protonated and deuterated methyl groups (see Figs. 24 and 25 for PI and PSF respectively). It must be stressed that even in the case of partial deuteration of all the hydrogens not belonging to the methyl group, identification of librational peaks is still a complicated task, since any other vibrational mode involving the motion of the methyl group hydrogens will provide a peak in the INS spectrum. A comparison with infrared and Raman measurements is helpful for a differentiation of the physical origin of the corresponding peaks. A nice example has been recently reported by Adams *et al.* for PIB and PI [147].

A relevant point for the analysis of librational features in INS spectra is the high sensitivity of the librational energies to the shape of the rotational barrier. Hence, the introduction of moderate sixfold corrections to the main threefold term of the rotational potential provides a significant shift of the librational energy. Figure 23b shows how the introduction of a small sixfold contribution is sufficient to account for the first librational peak of the ester-methyl group in PMMA [34], by using the same RRDM parameters describing both the rotational tunnelling and classical

hopping regimes. It is noteworthy that such a consistent description has been achieved by fixing a ratio $V_6/V_3 = 0.11$ for all the individual methyl groups. Hence, as in the purely threefold case, the only *independent* parameter affected by the distribution effects is the threefold term V_3 .

Librational energies are also sensitive to coupling between pairs of neighbouring methyl groups. In such cases, the single-particle approach is modified by introducing a coupling Hamiltonian. In the simplest approximation the coupling term is purely threefold and no angular offsets are included:

$$H = -B \left(\frac{\partial^2}{\partial \phi^2} + \frac{\partial^2}{\partial \psi^2} \right) + \frac{U_3}{2} (1 - \cos 3\phi) + \frac{V_3}{2} (1 - \cos 3\psi) + \frac{W_3^c}{2} (1 - \cos 3(\phi - \psi)). \quad (54)$$

In a recent INS investigation on methyl group librations in PSF [149], the double-peak structure in the range $\approx 34 - 44$ meV (see Fig. 25) has been interpreted as the result of a distribution of splitted first librational energies, such a splitting resulting from the coupling between the two methyl groups in each monomeric unit. As in the single-particle approach, the terms U_3 and V_3 are taken as Gaussian distributed. Due to the highly disordered character of the polymer matrix and the symmetric chemical arrangement of both methyl groups in the monomeric unit, it is expected that, on average, they feel the same typical environment. Hence, the distributions $g(U_3)$ and $g(V_3)$ are assumed to be identical. Since the coupling term W_3^c is strictly due to the interaction between the two methyl groups of the same monomeric unit, it is expected to be weakly affected by local packing conditions. Hence for simplicity, distribution effects are neglected for the coupling term.

The classical hopping regime for PSF is not accessible by QENS at low and moderate temperature, and at high temperature superposes with secondary relaxations which complicate the analysis. Instead, it can be properly explored by NMR techniques. Hence, the temperature dependence of the D-NMR line shape of PSF has been reproduced in terms of a log-Gaussian distribution of classical hopping frequencies as Eq. (44), with $\log \Gamma_0$ and σ respectively following Eqs. (45, 46). Analogously to the procedure exposed in Section IV, these results provide a Gaussian distribution of classical activation energies $f(E_A)$, which

can be transformed into a distribution of rotational barriers $g(V_3)$ and librational energies $F(E_{01})$ via the functional relations $E_A = E_A(V_3)$, $E_{01} = E_{01}(V_3)$. Such functional relations can be obtained by solving the eigenvalues of the Hamiltonian (54) for the selected value of W_3^c and a large set of values $U_3 = V_3$ (see Ref. [149] for numerical relations).

Fig. 25 shows the corresponding distributions $F(E_{01})$ for the single-particle approach, and for coupling of methyl groups, —with the conditions above explained for the second case. While the single-particle approach only gives account for the lowest experimental peak, the introduction of a coupling term reproduces the double-peak structure. Analogous results are obtained for PC and PH [149]. It is noteworthy that the introduction of a coupling term does not substantially complicate the original RRDM, since the only model parameter affected by the distribution effects is, as in the single-particle case, the rotational barrier height V_3 .

VII. MOLECULAR ORIGIN OF THE BARRIER DISTRIBUTION FOR METHYL GROUP DYNAMICS

The results summarized in Table II show that the average barrier height $\langle V_3 \rangle$ for methyl group reorientation in amorphous polymers is highly sensitive to the chemical structure of the monomeric unit. This fact suggests that the rotational potential is only partially determined by intermolecular interactions. On the other hand, there is not a clear correlation between the width of the barrier distribution and the chemical structure of the monomeric unit. Next we summarize the most relevant neutron scattering results relating the parameters of the barrier distribution with packing conditions and intermolecular interactions.

A. Influence of the chain conformation

The relative orientation between identical side groups placed at different monomeric units can be random or can adopt specific forms. Hence, in the *isotactic* (*i*) and *syndiotactic* (*s*) conformations, side groups at adjacent monomeric units are respectively parallel and anti-parallel. If both relative orientations

are randomly distributed, the conformation is *heterotactic* (*h*). When there is no dominating tacticity in the ensemble of chains forming the system, the latter is *atactic* (*a*). The ester-methyl group dynamics in PMMA have been analyzed in terms of the RRDM for different degrees of tacticity of the ester group. The influence of local packing conditions on the barrier distribution for samples chemically identical is evidenced by the small, but significant, differences between the obtained RRDM parameters [32,34,91,152] (see Table II). Hence, the average activation energy for a purely syndiotactic sample is $\langle E_A \rangle = 710$ K [34], while for an atactic sample with relation *s:i:h* = 50:10:40, $\langle E_A \rangle = 529$ K [91].

PMMA chains can be rearranged to form a stereocomplex form, where syndiotactic chains wrap around isotactic ones to form a double stranded helix structure. In Ref. [91] stereocomplexed samples with complementary deuteration of chains with different tacticities were investigated. In this way, the effect of stereocomplexation on methyl group dynamics in different types of chains could be discriminated. For the isotactic chains, stereocomplexation considerably reduced the width of $f(E_A)$, yielding a standard deviation $\sigma_E = 205$ K, as compared to the value $\sigma_E = 313$ K for the non-stereocomplexed sample [91].

For the case of the α -methyl group in PMMA, INS measurements showed a much higher librational peak [17], and consequently a much higher average rotational barrier, for the syndiotactic form as compared with the isotactic one. On the contrary, INS spectra for P α MS [17] did not show significant differences between a syndiotactic sample and an atactic one. FEW scans reported in Ref. [153] for different tacticities of PP did not show apparent differences, within the experimental noise, in the temperature range dominated by methyl group dynamics. This result is supported by the rather close values of the measured librational peaks for the isotactic [144] and atactic [145] conformations.

There are very few systems where experimental data are available for both, the usually investigated head-to-tail, and the head-to-head sequences of adjacent monomeric units. For P α MS [17] and for PP [111] it has been found, respectively by means of INS and QENS measurements, that the average barrier in the head-to-head conformation is much lower than in the head-to-tail one. In the case of hh-PP, the distribution

of classical activation energies $f(E_A)$ has been calculated from an analysis of high temperature data in terms of the hopping limit of the RRDM [111]. Apart from the mentioned decrease of the average barrier, the analysis provides a much narrower distribution than that obtained for head-to-tail PP [88,90]. It is worthy of remark that the maximum of the librational distribution $F(E_{01})$ for hh-PP, obtained by transformation from $f(E_A)$ in a purely threefold approach (see Section IV), is close to the experimental value reported in Ref. [145], though the agreement is not fully satisfactory [111]. A possible origin of such a difference might be, similarly to the case of the ester-methyl group in PMMA (see Section VI), the presence of small higher-order corrections to the main threefold term of the rotational potential, or small coupling effects between neighbouring methyl groups, which could shift the librational energy to slightly higher values than the expected ones for a purely threefold single-particle potential. This hypothesis is consistent with the proximity between methyl groups of adjacent units in the head-to-head conformation of PP.

B. Influence of mixing with other materials

A few works report comparisons between methyl group rotation in the neat polymer and blended with other polymers. QENS investigations in the blends PVME/PS [114,115] and hh-PP/PEO [111] did not show, for similar concentrations of the two components, changes within the error bar on the barrier distribution as compared respectively to neat PVME and hh-PP. High dilution of PVME in PVME/PS provided a significantly broader distribution, but again did not affect to the average barrier [115]. On the contrary, progressive dilution of PMMA in SCPE/PMMA increased the average barrier for the ester-methyl group even at moderate concentrations of SCPE [114].

The effect of doping with small molecules on methyl group dynamics has also been reported in the literature, though a detailed quantitative analysis in terms of barrier distributions is lacking. Hence, FEW scans in Ref. [110] showed no significant differences for neat PDMS and filled with silica nanoparticles. Some investigations on polymer electrolytes suggest that methyl group dynamics are not significantly affected by addition of the salt [119,120,128], but the present informa-

tion is rather limited to make reliable conclusions at a quantitative level.

C. Molecular glasses and comparison with the crystalline state

It is worthy of remark that, not only amorphous polymers, but also the low-molecular-weight glasses investigated until now display a similar phenomenology for methyl group dynamics. In contrast to amorphous polymers, glass-forming molecular systems can be easily obtained in the crystalline state. This possibility allows one to make a direct comparison between the methyl group dynamic features in the crystalline and glassy states of a same system. This comparison was done *in situ* for a same sample of sodium acetate trihydrate [36]. The analysis of the neutron scattering spectra, in the crystalline and glassy states, unambiguously demonstrated that the apparently quasielastic intensity observed for methyl group tunnelling in the glassy state is a consequence of the atomic disorder. Fig. 26 shows the corresponding tunnelling spectra for the crystalline and glassy state of sodium acetate trihydrate. For this system it was found that the average potential barrier in the glassy state takes, within the experimental error, the same value as the unique barrier in the crystal. A direct comparison between methyl group dynamics in the crystalline and glassy state has also been reported for ethylbenzene [154]. Disorder effects are evidenced by the broad structure of the librational peak in the glassy state as compared to the resolution-width line in the crystalline case. The small shift of the experimental maximum indicates that, as in sodium acetate trihydrate, the distribution is centered around the unique barrier of the crystal. On the contrary, an investigation on glassy toluene has reported an average rotational barrier much larger than the unique one of the crystalline state [35].

The widths of the barrier distributions obtained for the former molecular glasses take values comparable to those obtained for polymer glasses. All these results strongly suggest that the origin of the distribution of potential barriers in polymers is directly related to the structural disorder and packing conditions, and not with chain connectivity aspects which are specific of polymer glasses. This hypothesis has been recently

supported by measurements of the tunnelling spectrum of tri(vinyl acetate) [143]. As can be seen in Fig. 27, the experimental spectrum at $T = 2$ K is reproduced by using the same RRDM parameters as in PVAc, suggesting that the barrier distribution is not affected by polymerization of the basic molecular unit.

D. Molecular dynamics simulations

A deep understanding of the microscopic origin of the distribution of potential barriers is not easily inferred from experiments. However, fully atomistic MDS are a suitable tool to gain insight into this problem. In particular, the calculation of the distribution of librational energies is straightforward and does not require lengthy simulation runs. As has been exposed in previous Sections, once this distribution is obtained, the corresponding distribution of potential barriers can be directly derived by transformation of the former. In addition, MDS offer the possibility of varying the parameters of the employed force field, and to investigate the influence of the modified force field on methyl group dynamics. A comparison between MDS and neutron scattering results on PI was reported in Ref. [87]. From the atomic trajectories computed in the simulations, the generalized VDOS, $Z(\omega)$, was calculated as the spectral density of the velocity autocorrelation function:

$$Z(\omega) \propto \int_0^\infty e^{-i\omega t} \langle \varrho \mathbf{v}(t) \cdot \mathbf{v}(0) \rangle dt, \quad (55)$$

where brackets denote ensemble average over all the atoms. The weighting factor ϱ contains, for each atomic species, the corresponding cross-section and mass, in order to make a direct comparison with the experimental results. Fig. 28 shows a comparison between the INS data reported by Frick and Fetters [26] for PI-d5 (deuterated main-chain and protonated methyl group) and the generalized VDOS, computed from the MDS as in Eq. (55). A good agreement is obtained at least in the energy range, $\hbar\omega \lesssim 40$ meV, experimentally investigated in Ref. [26], validating the employed force field. Although quantum effects (not considered in the classical MDS) should certainly affect the high energy range of $Z(\omega)$, it is worthy of remark that the energies of the computed high energy

maxima (see Fig. 28) roughly correspond to the reported infrared and Raman bands [155], as well as to recent INS results by Adams *et al* [147].

It must be reminded that, although the generalized VDOS for PI-d5 is dominated by motions of methyl group protons, it contains not only the contributions of the librational modes, but also from any other mode involving the motion of the methyl group. This is evidenced in Fig. 24, where the librational peak is superimposed to a broad low-energy hump similar to that present in the generalized VDOS of PI-d3 (deuterated methyl group and protonated main-chain). However, the methyl group librational contribution can be separated from the computed generalized VDOS by calculating the spectral density of the angular correlation function [87]:

$$F(E_{01}) \propto \int_0^\infty e^{-iE_{01}t} \langle \dot{\phi}(t) \dot{\phi}(0) \rangle dt, \quad (56)$$

where brackets denote ensemble average *over methyl group protons*. $F(E_{01})$ is formally the librational density of states. Finally, the distribution of potential barriers $g(V_3)$ is obtained by transformation from $F(E_{01})$ as exposed in Section IV.

In order to investigate the relation between the average and width of the barrier distribution and the non-bond interactions, a series of MDS were carried out with different values of the cutoff radius, r_c , for the nonbond interactions of the employed force field. The cutoff r_c was changed from 11 Å (the value for realistic conditions) to 4 Å. Simulations were also performed for the isolated chain. The results reported in Ref. [87] are summarized in Fig. 29. Diminishing the cutoff radius yields a systematic decrease of the average barrier and the width of the barrier distribution $g(V_3)$. An abrupt change of the latter parameters takes place in a narrow region around $r_c \approx 5$ Å, which roughly corresponds to the inter-macromolecular distances in PI. This result suggests that only the nonbond interactions at the inter-chain distances play a significant role in determining the width of the distribution of rotational barriers for methyl group rotation. Moreover, it is worthy of remark that these interactions also affect significantly to the average value of the potential barrier, i.e., the latter is not only determined by the chemical structure of the monomeric unit.

VIII. CONCLUSIONS AND OUTLOOK

This paper gives a comprehensive review of neutron scattering investigations on methyl group dynamics in glassy polymers of different chemical composition and microstructure. Considerable progress on this topic has been achieved over last 10 years mainly fueled by two facts: (i) the proposal in 1994 of the Rotation Rate Distribution Model for methyl group dynamics in polymers; (ii) the first direct experimental observation in 1998 by neutron scattering of quantum rotational tunnelling in glassy polymers at very low temperature.

The experimental data presented in this paper demonstrate the uniqueness, the power, and the efficiency of the combination of quasielastic and inelastic neutron scattering for investigating this problem. In particular, it is worthy of remark that neutron scattering is the only technique which provides a direct experimental observation of quantum tunnelling processes of methyl groups. There are, however, some limitations, mainly related to the current resolution of the available high-resolution backscattering spectrometers (≈ 0.3 μeV), which prevents the observation of clear rotational tunnelling features at very low temperature in polymers when the average rotational barrier is higher than ≈ 1000 K.

On the other hand, in this article it is shown that distribution effects are essential to understand methyl group dynamics—from quantum tunnelling to classical hopping—in polymeric materials and in other highly disordered systems as well. The Rotation Rate Distribution Model (RRDM), which introduces a distribution of potential barriers for methyl group rotation, provides a consistent description for the experimental features observed at different temperatures, including the crossover from quantum to classical behavior and the librational energies as well.

Taking into account the RRDM results on different polymer systems as well as on low molecular weight glasses, it is now evident that the distribution of potential barriers is determined by the intermolecular disorder and that the chain connectivity does not play any significant role. However, apart from these qualitative results, it is clear that the actual origin of the distribution of potential barriers and its possible relationship with the structure factor characterizing the packing conditions, is one of the main points that still needs to be clarified. Concerning this question, fully

atomistic molecular dynamics simulations can play an important role in the near future. The results available by now suggest that the width of the distribution of potential barriers is mainly determined by the nonbond interactions at the inter-chain distances, at least in the case of polyisoprene. These results need to be confirmed by similar simulations in other realistic model systems as for instance, PMMA.

Another way of addressing this question experimentally would be to carry out neutron scattering measurements on methyl group dynamics in polymers under confinement conditions, and to compare them with the corresponding results for the bulk state. To the best of our knowledge, a quantitative determination of the barrier distribution for methyl group rotation has never been reported for a confined polymer. However, this has been recently carried out for glassy toluene confined in mesoporous silicates [94]. From the knowledge of the barrier distribution in the bulk glassy state [35], and by investigating the dependence of the RRDM parameters on the monodisperse radius of the confining pores, a lower limit has been estimated for the distance beyond which methyl groups do not feel the interaction with the pore wall and behave as bulk-like rotors. This procedure has confirmed that the interaction range relevant for methyl group dynamics in glassy toluene extends beyond the typical nearest-neighbour distance between centers-of-mass [94]. Similar investigations on confined polymers would be helpful to improve our understanding of the structural origin of the barrier distribution for methyl group rotation in polymers.

ACKNOWLEDGEMENTS

We are grateful to all colleagues with whom we have had the pleasure of collaborating on this topic over last years: C. Alba-Simionesco, J.M. Alberdi, F. Alvarez, A. Arbe, A. Chahid, G. Dosseh, D. Fernández, B. Frick, A.C. Genix, H. Grimm, D. Morineau, R. Mukhopadhyay, R. Pérez, M. Prager, D. Richter, M. Tyagy, and L. Willner. We also thank M. Tyagy for sharing his unpublished results on PDMS and tri(vinyl acetate). We acknowledge experimental facilities from ILL (Grenoble, France), IFF (Jülich, Germany), and ISIS (Chilton, United Kingdom).

-
- [1] McCrum NG, Read BE, Williams G. Anelastic and dielectric effects in polymer solids. New York, NY: Wiley, 1967.
 - [2] Bailey RT, North AM, Pethrick RA. Molecular motion in high polymers. Oxford, United Kingdom: Clarendon Press, 1981.
 - [3] Doi M, Edwards SF. The Theory of Polymer Dynamics. Oxford, United Kingdom: Oxford University Press, 1986.
 - [4] Richter D, Monkenbusch M, Arbe A, Colmenero J. Neutron spin echo in polymer systems. *Adv Polym Sci* 2005;174:1-221.
 - [5] Prager M, Heidemann A. Rotational tunneling and neutron spectroscopy: A compilation. *Chem Rev* 1997;97:2933-2966.
 - [6] Press W. Single Particle Rotations in Molecular Crystals. Springer Tracts in Modern Physics 92. Berlin, Germany: Springer, 1981.
 - [7] Carlile CJ, Prager M. Rotational tunneling spectroscopy with neutrons. *Int J Mod Phys B* 1993;7:3113-3151.
 - [8] Abramowitz M, Segun IA. Handbook of mathematical functions. New York, NY: Dover, 1968.
 - [9] Hüller A. Temperature dependence of rotational tunnelling. *Z Phys B* 1980;36:215-225.
 - [10] Clough S, Heidemann A, Horsewill AJ, Lewis JD, Paley MNJ. The rate of thermally activated methyl group rotation in solids. *J Phys C* 1982;15:2495-2508.
 - [11] Hewson AC. The temperature dependence of inelastic neutron scattering in rotational tunnelling systems. I. Formulation and perturbation theory. *J Phys C* 1982;15:3841-3853.
 - [12] Hewson AC. The temperature dependence of inelastic neutron scattering in rotational tunnelling systems. II. Calculation of the time-dependent correlation functions. *J Phys C* 1982;15:3855-3867.
 - [13] Würger A. The temperature dependence of rotational tunnelling. *Z Phys B* 1989;76:65-76.
 - [14] Clough S, Horsewill AJ, Johnson MR. Approximate topology and the nonexistence of spin-symmetry species of hindered methyl groups. *Phys Rev A* 1993;47:3420-3423.
 - [15] Horsewill AJ. Quantum tunnelling aspects of methyl group rotation studied by NMR. *Prog Nucl Mag Reso Sp* 1999;35:359-389.
 - [16] Higgins JS, Allen G, Brier PN. Methyl group motion in poly(propylene oxide), polypropylene and poly(methyl methacrylate). *Polymer* 1972;13:157-

- 163.
- [17] Allen G, Wright CJ, Higgins JS. Effect of polymer microstructure on methyl group torsional vibrations. *Polymer* 1974;15:319-322.
- [18] Connor TM. Distributions of correlation times. Their effect on comparison of molecular motions derived from nuclear spin-lattice and dielectric relaxation. *T Faraday Soc* 1964;60:1574-1580.
- [19] Schmidt C, Kuhn KJ, Spiess HW. Distribution of correlation times in glassy-polymers from pulsed deuteron NMR. *Progr Coll Pol Sci* 1985;71:71-76.
- [20] Gabrys B, Higgins JS, Ma KT, Roots JE. Rotational motion of the ester methyl group in stereoregular poly(methyl methacrylate). A neutron scattering study. *Macromolecules* 1984;17:560-566.
- [21] Gabrys B, Higgins JS, Young DA. Rotation of methyl groups in molecular solids and polymers at low temperatures. Recent developments. *Polymer* 1985;26:355-363.
- [22] Floudas G, Higgins JS. Ester methyl group rotation in poly(methyl methacrylate) and in the blend solution chlorinated polyethylene/poly(methyl methacrylate). A quasielastic neutron scattering study. *Polymer* 1992;33:4121-4128.
- [23] Arrighi V, Higgins JS, Burgess AN, Howells WS. Rotation of methyl side groups in polymers: A Fourier transform approach to quasielastic neutron scattering. 1. Homopolymers. *Macromolecules* 1995;28:2745-2753.
- [24] Arrighi V, Higgins JS. Side group rotations in amorphous polymers. *Physica B* 1996;226:1-9.
- [25] Chahid A, Alegría A, Colmenero J. Methyl group dynamics in poly(vinyl methyl ether): A rotation rate distribution model. *Macromolecules* 1994;27:3282-3288.
- [26] Frick B, Fetters LJ. Methyl group dynamics in glassy polyisoprene: A neutron backscattering investigation. *Macromolecules* 1994;27:974-980.
- [27] Chahid A, Colmenero J, Alegría A. Fast dynamics below and around the glass-transition in a sidegroup polymer (PVME). *Physica A* 1993;201:101-105.
- [28] Hoch MJR, Bovey FA, Davis DD, Douglass DC, Falcone DR, McCall DW, Slichter WP. Nuclear magnetic resonance in poly(vinyl acetate). *Macromolecules* 1971;4:712-715
- [29] Williams J, Shohamy E, Reich S, Eisenberg A. Methyl group tunneling in viscoelastic relaxation: Experimental verification. *Phys Rev Lett* 1975;35:951-953.
- [30] Williams J, Eisenberg A. Methyl group tunneling and viscoelastic relaxation in poly(methyl methacrylate). *Macromolecules* 1978;11:700-707.
- [31] Colmenero J, Mukhopadhyay R, Alegría A, Frick B. Quantum rotational tunneling of methyl groups in polymers. *Phys Rev Lett* 1998;80:2350-2353.
- [32] Moreno AJ, Alegría A, Colmenero J, Frick B. Isotope effect on the rotational tunneling transitions of methyl groups in glassy polymers. *Phys Rev B* 1999;59:5983-5986.
- [33] Moreno AJ, Alegría A, Colmenero J. Methyl group dynamics in glassy systems: Crossover from quantum to classical regime. *Phys Rev B* 2001;63:R60201(1-4).
- [34] Moreno AJ, Alegría A, Colmenero J, Frick B. Methyl group dynamics in poly(methyl methacrylate): From quantum tunneling to classical hopping. *Macromolecules* 2001;34:4886-4896.
- [35] Moreno AJ, Alegría A, Colmenero J, Prager M, Grimm H, Frick B. Methyl group dynamics in glassy toluene: A neutron scattering study. *J Chem Phys* 2001;115:8958-8966.
- [36] Moreno AJ, Alegría A, Colmenero J, Frick B. Methyl group dynamics from tunneling to hopping in $\text{NaCH}_3\text{CO}_2 \cdot 3\text{H}_2\text{O}$: Comparison between a crystal and its glassy counterpart. *Phys Rev B* 2002;65:134202(1-10).
- [37] Bée M. *Quasielastic Neutron Scattering: Principles and Applications in Solid State Chemistry, Biology and Materials Science*. Bristol, United Kingdom: Adam Hilger, 1988.
- [38] Springer T. *Quasielastic Neutron Scattering for the Investigation of Diffusive Motions in Solids and Liquids*. Berlin, Germany: Springer-Verlag, 1972.
- [39] Lovesey SW. *Theory of Neutron Scattering from Condensed Matter*. International Series of Monographs on Physics. Oxford, United Kingdom: Clarendon Press, 1984.
- [40] Squires GL. *Introduction to the Theory of Thermal Neutron Scattering*. New York, NY: Dover, 1996.
- [41] <http://www.ill.fr/YellowBook/IN5/>.
- [42] <http://www.ill.fr/YellowBook/IN6/>.
- [43] <http://www.ill.fr/YellowBook/IN16/>.
- [44] <http://www.ill.fr/YellowBook/D7/>.
- [45] Schärpf O, Capellmann H. The XYZ-difference method with polarized neutrons and the separation of coherent, spin incoherent, and magnetic scattering cross sections in a multidetector. *Phys Stat Sol A* 1993;135:359-379.
- [46] <http://www.isis.rl.ac.uk/molecularspectroscopy/tosca/>
- [47] Batley M, Thomas RK, Heidemann A, Overs AH, White JW. Methyl group tunnelling and torsion in 2,4-hexadiyne. *Mol Phys* 1977;34:1771-1778.
- [48] Prager M, Duprée KH, Müller-Warmuth W. Rotational tunneling and methyl group reorientation in tetramethyltin $[\text{Sn}(\text{CH}_3)_4]$ by inelastic neutron scattering and nuclear magnetic resonance. *Z Phys B*

- 1983;51:3090-3098.
- [49] Cavagnat D, Lascombe J, Lassegues JC, Horsewill AJ, Heidemann A, Suck JB. Neutron and Raman scattering studies of the methyl dynamics in solid toluene and nitromethane. *J Physique (Paris)* 1984;45:97-105.
- [50] Heidemann A, Prager M, Monkenbusch M. Methyl rotation in acetamide: the transition from quantum mechanical tunneling to classical reorientation studied by inelastic neutron scattering. *Z Phys B* 1989;76:77-88.
- [51] Emid S. On the symmetry of the rotor part of the rotor-phonon interaction of reorienting or tunnelling molecular groups in solids. *Chem Phys Lett* 1980;72:189-193.
- [52] Clough S, Heidemann A. A study of the temperature dependence of a methyl tunnelling spectrum by inelastic neutron scattering. *J Phys C* 1979;12:761-770.
- [53] Clough S, Heidemann A, Paley M. The temperature dependence of methyl tunnelling motion in three acetates. *J Phys C* 1981;14:1001-1008.
- [54] Cockbain JR, Lechner R, Owen M, Thomas RK, White JW. Methyl group rotation in hexadiyne. II. The transition from classical to quantum dynamics. *Mol Phys* 1982;45:1035-1051.
- [55] Cavagnat D, Magerl A, Vettier C, Clough S. Methyl tunnelling in α -crystallised toluene by inelastic neutron scattering: Temperature and pressure effects *J Phys C* 1986;19:6665-6672.
- [56] Prager M, Langel W. Intermolecular interaction in $\text{Sn}(\text{CH}_3)_4$: An inelastic neutron scattering study of matrix isolated molecules. *J Chem Phys* 1986;85:5279-5285.
- [57] Prager M, Stanislawski J, Häusler W. Inelastic incoherent neutron scattering study of the methyl rotation in various methyl halides. *J Chem Phys* 1987;86:2563-2575.
- [58] Prager M. Methyl quantum rotation in solid CH_3F : An inelastic neutron scattering study *J Chem Phys* 1988;89:1181-1184.
- [59] Prager M, Hempelmann R, Langen H, Müller-Warmuth W. Methyl tunneling and rotational potentials in solid xylenes and fluorotoluenes. *J Phys: Condens Matter* 1990;2:8625-8638.
- [60] Allen PS. A model for a temperature dependent frequency distribution of methyl group tunnelling splittings. *J Phys C* 1974;7:L22-L25.
- [61] Punkkinen M. Temperature dependence of the librational tunneling and proton relaxation. *Phys Rev B* 1980;21:54-60.
- [62] Clough S, Heidemann A. The approach to classical dynamics of reorienting methyl groups. *J Phys C* 1980;13:3585-3589.
- [63] Clough S. The response of a tunnelling particle to an impulse. *J Phys C* 1985;18:L1-L4.
- [64] Whittall MWG, Gehring GA. Path integral approach to methyl group rotation. *J Phys C* 1987;20:1619-1639.
- [65] Clough S, Horsewill AJ, Johnson MR. Approximate rotational quantization and the Pauli principle. *Chem Phys Lett* 1993;208:143-147.
- [66] Clough S. Methyl group hopping reorientation and the non-existence of spin symmetry species at room temperature. *Chem Phys Lett* 1981;80:389-392.
- [67] Emid S. Existence of spin symmetry species in reorienting methyl groups at high temperatures *Chem Phys Lett* 1981;80:393-397.
- [68] Clough S. A kinetic theory of the temperature dependence of methyl tunnelling spectra. *J Phys C* 1981;14:1009-1024.
- [69] Gunn JMF. Comment on "The response of a tunnelling particle to an impulse". *J Phys C* 1985;18:L357-L362.
- [70] Clough S. The response of a tunnelling particle to an impulse: The connection with Berry's phase. *J Phys C* 1987;20:5905-5906.
- [71] Hüller A, Baetz L. Rotational tunnelling: A computer simulation at finite temperature. *Z Phys B* 1988;72:47-54.
- [72] Würger A. Rotational tunnelling and Kramers degeneracy. *J Phys: Condens Matter* 1989;1:1673-1675.
- [73] Würger A. The temperature dependence of inelastic rotational tunnelling transitions. *J Phys: Condens Matter* 1989;1:6901-6905.
- [74] Clough S. The topology of methyl rotation and gauge theory in solids. *Mol Phys* 1989;68:1255-1263.
- [75] Hüller A. Rotational tunneling at finite temperatures: Substitution by an equivalent harmonic system. *Z Phys B* 1990;78:125-129.
- [76] Würger A, Hüller A. Rotational Tunneling: The width of the quasielastic line. *Z Phys B* 1990;78:479-484.
- [77] Würger A. High temperature quantum effects in methyl rotation. *Z. Phys. B* 1991;84:263-267.
- [78] Braun D, Weiss U. Dynamics of the damped rotational tunneling system: The effect of librational excitations. *Z Phys B* 1993;92:507-517.
- [79] Vowe A. The temperature dependence of rotational tunneling, modeled with a harmonic substitute system. *J Phys: Condens Matter* 1993;5:8531-8544.
- [80] Clough S, Horsewill AJ, Alsanooi AM, Barlow MJ, Johnson MR. The spectrum of rotating wavepackets of hindered methyl groups. *Chem Phys Lett* 1993;211:637-642.
- [81] Clough S. The rotational spectrum of tunneling methyl groups. *Z Naturforsch A* 1994;49:1193-1199.

- [82] Braun D, Weiss U. Rotational tunneling and librational excitations: The loss of quantum coherence. *Physica B* 1994;202:264-272.
- [83] Clough S. Trajectories in methyl rotation. *Physica B* 1996;226:228-230.
- [84] Peternelj J. Rotational hopping model and decoherence. *Phys Rev B* 1999;60:3989-3994.
- [85] Nicholson TM, Davies GR. Modeling of methyl group rotations in PMMA. *Macromolecules* 1997;30:5501-5505.
- [86] Saelee C, Nicholson TM, Davies GR. A molecular dynamics study of methyl group rotation in poly(vinyl methyl ether). *Macromolecules* 2000;33:2258-2265.
- [87] Alvarez F, Alegría A, Colmenero J, Nicholson TM, Davies GR. Origin of the distribution of potential barriers for methyl group dynamics in glassy polymers: A molecular dynamics simulation in polyisoprene. *Macromolecules* 2000;33:8077-8084.
- [88] Ahumada O, Theodorou DN, Triolo A, Arrighi V, Karatasos C, Ryckaert JP. Segmental dynamics of atactic polypropylene as revealed by molecular simulations and quasielastic neutron scattering. *Macromolecules* 2002;35:7110-7124.
- [89] Mukhopadhyay R, Alegría A, Colmenero J, Frick B. Methyl group dynamics in poly(vinyl acetate): A neutron scattering study. *Macromolecules* 1998;31:3985-3993.
- [90] Arrighi V, Ferguson R, Lechner RE, Telling M, Triolo A. Local dynamics of atactic polypropylene across the glass transition. *Physica B* 2001;301:35-43.
- [91] Pillay R, Arrighi V, Kagunya W, Higgins JS. Ester methyl group dynamics in the poly(methyl methacrylate) stereocomplex: A neutron scattering study. *Macromolecular Symposia* 2001;166:269-276.
- [92] Zorn R, Frick B, Fetters LJ. Quasielastic neutron scattering study of the methyl group dynamics in polyisoprene. *J Chem Phys* 2002;116:845-853.
- [93] Arrighi V, Gagliardi S, Zhang CH, Ganazzoli F, Higgins JS, Ocone R, Telling MTF. A unified picture of the local dynamics of poly(dimethylsiloxane) across the melting point. *Macromolecules* 2003;36:8738-8748.
- [94] Moreno AJ, Colmenero J, Alegria A, Alba-Simionesco C, Dosseh G, Morineau D, Frick B. Methyl group dynamics in a confined glass. *Eur Phys J E* 2003;12:S43-S46.
- [95] Prager M, Heidemann A, Häusler W. Coupled pairs of quantum rotors in dichlorodimethylstannane: An inelastic neutron scattering study. *Z Phys B* 1986;64:447-452.
- [96] Heidemann A, Eckert J, Passell L, Häusler W. Pressure dependence of tunneling and librational modes of coupled methyl groups in lithium acetate. *Z Phys B* 1987;66:75-81.
- [97] Heidemann A, Friedrich H, Günter E, Häusler W. Tunneling of coupled methyl groups in lithium acetate: the isotope effect. *Z Phys B* 1989;76:335-344.
- [98] Fillaux F, Carlile CJ. Inelastic neutron scattering study of methyl tunneling and the quantum sine-Gordon breather in isotopic mixtures of 4-methylpyridine at low temperature. *Phys Rev B* 1990;42:5990-6006.
- [99] Fillaux F, Carlile CJ, Kearley GJ, Prager M. Inelastic neutron scattering study of methyl tunneling and the quantum sine-Gordon breather mode in isotopic mixtures of 2,6-dimethylpyridine at low temperature. *Physica B* 1994;202:302-310.
- [100] Fillaux F, Carlile CJ, Kearley GJ. Inelastic neutron scattering study of the sine-Gordon breather interactions in isotopic mixtures of 4-methylpyridine. *Phys Rev B* 1998;58:11416-11419.
- [101] Alvarez F, Alegría A, Colmenero J. A new method for obtaining distributions of relaxation-times from frequency relaxation spectra. *J Chem Phys* 1995;103:798-806.
- [102] Karatasos K, Ryckaert JP, Ricciardi R, Laupretre F. Methyl dynamics and beta-relaxation in polyisobutylene: Comparison between experiment and molecular dynamics simulations. *Macromolecules* 2002;35:1451-1462.
- [103] Tyagi M, Alegría, Colmenero J. Heterogeneous dynamics in poly(vinyl acetate) far above T_g : A combined study by dielectric spectroscopy and quasielastic neutron scattering. *J Chem Phys*, in press.
- [104] Arrighi V, Higgins JS, Floudas G, Borgess AN. Effect of blending on polymer chain dynamics. In: Colmenero J, Alegría A, Bermejo FJ editors. *Quasielastic Neutron Scattering. Future prospects on high resolution inelastic neutron scattering*. Singapore: World Scientific, 1994. p. 164-173.
- [105] Allen G, Higgins JS. Verification of long-range and localized dynamics of molecules in an amorphous polymer matrix. *Macromolecules* 1977;10:1006-1010.
- [106] Chahid A, Alegría A, Colmenero J. Distribution of the activation energy for methyl side group rotation in poly(vinyl methyl ether). In: Colmenero J, Alegría A, Bermejo FJ editors. *Quasielastic Neutron Scattering. Future prospects on high resolution inelastic neutron scattering*. Singapore: World Scientific, 1994. p. 227-235.
- [107] Frick B. Methyl groups dynamics in poly(dimethyl siloxane). In: Giordano M, Leporini D, Tosi MP editors. *Non-Equilibrium phenomena in supercooled fluids, glasses and amorphous materials*. Singapore: World Scientific, 1996. p255-256.
- [108] Grapengeter HH, Alefeld B, Kosfeld R. An investi-

- gation of micro-Brownian motions in polydimethylsiloxane by complementary incoherent neutron scattering and NMR experiments below room temperature. *Colloid Polym Sci* 1987;265:226-233.
- [109] Arrighi V, Ganazzoli F, Zhang C, Gagliardi S. New interpretation of local dynamics of poly(dimethyl siloxane) observed by quasielastic neutron scattering. *Phys Rev Lett* 2003;90:058301(1-4).
- [110] Arrighi V, Higgins JS, Burgess AN, Floudas G. Local dynamics of poly(dimethyl siloxane) in the presence of reinforcing filler particles. *Polymer* 1998;39:6369-6376.
- [111] Pérez R, Arbe A, Colmenero J, Willner L, Richter D, Frick B. Quasielastic neutron scattering study on the effect of blending on the dynamics of head-to-head poly(propylene) and poly(ethylene propylene). Submitted.
- [112] Schonhals A, Goering H, Schick C, Frick B, Zorn R. Glass transition of polymers confined to nanoporous glasses. *Colloid Polym Sci* 2004;282:882-891.
- [113] Floudas G, Higgins JS. Quasielastic neutron scattering from a polymer blend in the one- and two-phase region. *Physica B* 1992;182:361-364.
- [114] Arrighi V, Higgins JS, Burgess AN, Howells WS. Rotation of methyl side groups in polymers: A Fourier transform approach to quasielastic neutron scattering. 2. Polymer blends. *Macromolecules* 1995;28:4622-4630.
- [115] Mukhopadhyay R, Alegría A, Colmenero J, Frick B. Effect of blending on the methyl side group dynamics in poly(vinyl methyl ether). *J Non-Cryst Solids* 1998;235:233-236.
- [116] Genix AC, Arbe A, Alvarez F, Colmenero J, Willner L, Richter D. The dynamics of poly(ethylene oxide) in a blend with poly(methyl methacrylate). A quasielastic neutron scattering and molecular dynamics simulations study. Submitted
- [117] Maranas JK *et al.*, submitted.
- [118] Soles CL, Douglas JF, Lin EK, Lenhart JL, Jones RL, Wu WL. Incoherent neutron scattering and the dynamics of thin film photoresist polymers. *J Appl Phys* 2003;93:1978-1986.
- [119] Carlsson P, Mattsson B, Swenson J, Torell LM, Käll M, Börjesson L, McGreevy RL, Mortensen K, Gabrys B. Neutron scattering studies of a polymer electrolyte, PPO-LiClO₄. *Solid State Ionics* 1998;113:139-147.
- [120] Andersson D, Carlsson P, Engberg D, Torell LM, Börjesson L, McGreevy RL, Howells WS. Modelling of segmental dynamics in polymer electrolyte PPO-LiClO₄, by surface fitting of quasi-elastic neutron scattering data. *Physica B* 1999;266:126-130.
- [121] Karlsson C, Best AS, Swenson J, Howells WS, Börjesson L. Polymer dynamics in 3PEG-LiClO₄-TiO₂ nanocomposite polymer electrolytes. *J Chem Phys* 2003;118:4206-4212.
- [122] Fitter J, Adams M, Coddens G, Buldt G, Dencher NA and Lechner RE. Dynamical structure and function of purple membrane as seen by neutrons. *Physica B* 1995;213:775-779.
- [123] Arrighi V, Higgins JS. Molecular dynamics of a main-chain liquid crystalline polyester below the crystalline to nematic phase transition. *J Chem Soc Faraday T* 1997;93:1605-1612.
- [124] Arrighi V, Higgins JS, Mani S, Stoeber L. Molecular dynamics of main-chain liquid crystalline polymers. *Physica B* 1999;266:1-12.
- [125] Swenson J, Koper I, Telling MTF. Dynamics of propylene glycol and its 7-mer by neutron scattering. *J Chem Phys* 2002;116:5073-5079.
- [126] Swenson J, Howells WS. Quasielastic neutron scattering of propylene glycol and its 7-mer confined in a clay. *J Chem Phys* 2002;117:857-865.
- [127] Swenson J, Engberg D, Howells WS, Seydel T, Juranyi F. Dynamics of propylene glycol and its oligomers confined to a single molecular layer. *J Chem Phys* 2005;122:244702(1-9).
- [128] Russina O, Triolo A, Aihara Y, Telling MTF, Grimm H. Quasielastic neutron scattering investigation of dynamics in polymer electrolytes. *Macromolecules* 2004;37:8653-8660.
- [129] Alvarez F, Arbe A, Colmenero J. Methyl group dynamics above the glass transition temperature: A molecular dynamics simulation in polyisoprene. *Chem Phys* 2000;261:47-59.
- [130] Prager M, Schiebel P, Combet J. Rotational tunnelling and molecular disorder of 4-iodo-toluene. *Chem Phys* 2002;276:69-79.
- [131] Prager M, Pieper J, Buchsteiner A, Desmedt A. Probing adsorption sites in a cubic II water clathrate cage by methyl group rotation of CH₃I guest molecules. *J Phys: Condens Matter* 2004;16:7045-7061.
- [132] Nair S, Dimeo RM, Neumann DA, Horsewill AJ, Tsapatsis M. Methyl rotational tunneling dynamics of p-xylene confined in a crystalline zeolite host. *J Chem Phys* 2004;121:4810-4819.
- [133] Leclercq F, Damay P, Chieux P. Neutron scattering investigation of the structure, phase stability, and rotational excitations in the compounds Ca(NH₃)_n and Ca(ND₃)_n as a function of composition (5 < n ≤ 6.5). *J Phys Chem* 1990;94:7300-7308.
- [134] Margadonna S, Prassides K, Brown CM, Shimoda H, Iwasa Y, Casalta H. Rotational tunneling of ammonia in (NH₃)K₃C₆₀. *J Chem Phys* 1999;111:10969-10973.

- [135] Asmussen B, Press W, Prager M, Blank H. Rotational excitations in CH₄ krypton mixtures. *J Chem Phys* 1993;98:158-163.
- [136] Prager M and Langel W. Rotational excitations of methane molecules in a nonequilibrium krypton matrix. *J Chem Phys* 1989;90:5889-5890.
- [137] Prager M, Asmussen B and Carlile CJ. Methane in neon. Nearly free rotation in a mismatched guest-host system. *J Chem Phys* 1994;100:247-251.
- [138] Bostoen C, Coddens G, Wegener W. Rotational excitations in K_{1-x}(NH₄)_xI mixed crystals: A neutron scattering study. *J Chem Phys* 1989;91:6337-6344.
- [139] Mukhopadhyay R, Narasimhan SL. Rotational excitations of NH₄⁺ ions in metal alkali halide lattices. Are they strain field mediated?. *Solid State Commun* 1995;94:461-464.
- [140] Dimeo RM, Neumann DA. Low-temperature dynamics of confined methyl iodide. *Phys Rev B* 2001;63:14301(1-9).
- [141] Dimeo RM, Neumann DA. The effects of confinement on rotational tunneling. *Appl Phys A* 2002;74:S1382-S1384.
- [142] Dimeo RM, Neumann DA, Glanville Y, Minor DB. Pore size dependence of rotational tunneling in confined methyl iodide. *Phys Rev B* 2002;66:104201(1-5).
- [143] Tyagy M *et al.*, unpublished results.
- [144] Takeuchi H, Higgins JS, Hill A, Maconnachie A, Allen G, Stirling GC. Investigation of the methyl torsion in isotactic polypropylene. Comparison between neutron inelastic scattering spectra and normal coordinate calculations. *Polymer* 1982;23:499-504.
- [145] Annis BK, Lohse DJ, Trouw F. Observation of boson peaks by inelastic neutron scattering in polyolefins. *J Chem Phys* 1999;111:1699-1704.
- [146] Mukhopadhyay R, Colmenero J, Alegría A, Moreno AJ. Methyl group librations in glassy polymers. *ISIS Exp Rep No 9638* (2000).
- [147] Adams MA, Gabrys BJ, Zajac WM, Peiffer DG. High-resolution incoherent inelastic neutron scattering spectra of polyisobutylene and polyisoprene. *Macromolecules* 2005;38:160-166.
- [148] Frick B, Richter D, Trevino S. Inelastic fast relaxation in a weakly fragile polymer glass near T_g . *Physica A* 1993;201:88-94.
- [149] Fernández D *et al.*, submitted.
- [150] Kubota H, Kaneko F, Kawaguchi T. Study of thermodynamic stabilities of polytypes of n -C₃₆H₇₄ by solubility measurements and incoherent inelastic neutron scattering. *J Chem Phys* 2005;122:024903(1-6).
- [151] Frick B. *Polymer Motions in Dense Systems*. Richter D, Springer T, eds. (Springer-Verlag, Berlin 1988).
- [152] Cereghetti PM, Kind R, Higgins JS. Tacticity effects on the barriers to rotation of the ester methyl group in poly(methyl methacrylate): A deuteron magnetic resonance study. *J Chem Phys* 2004;121:8068-8078.
- [153] Arrighi V, Batt-Coutrot D, Zhang CH, Telling MTF, Triolo A. Effect of tacticity on the local dynamics of polypropylene melts. *J Chem Phys* 2003;119:1271-1278.
- [154] Frick B, Williams J, Trevino S, Erwin R. Vibrational behavior of amorphous and crystalline ethylbenzene. *Physica B* 1995;213:506-509.
- [155] Mark JE editor. *Physical Properties of Polymers Handbook*. New York: AIP, 1996.

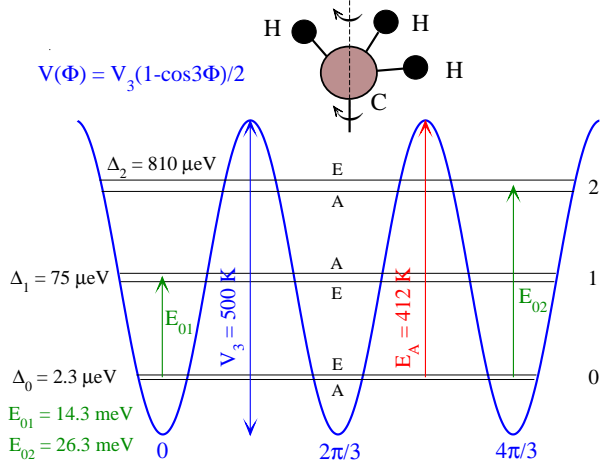


FIG. 1. Picture of methyl group rotation about its C_3 -axis, and level scheme for a purely threefold potential with barrier height $V_3 = 500$ K.

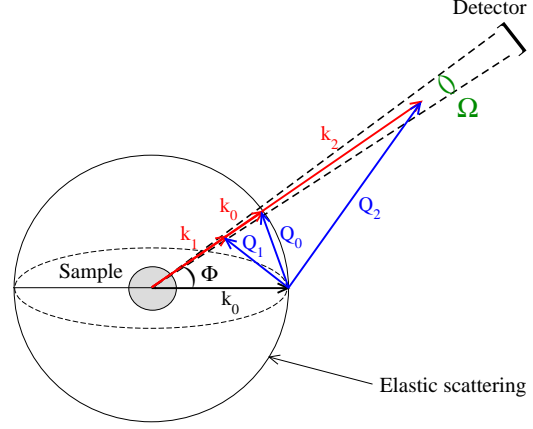


FIG. 2. Scheme of a scattering experiment. The sphere of radius k_0 represents elastic interactions. Indexes 1 and 2 respectively correspond to inelastic processes with neutron energy loss and gain.

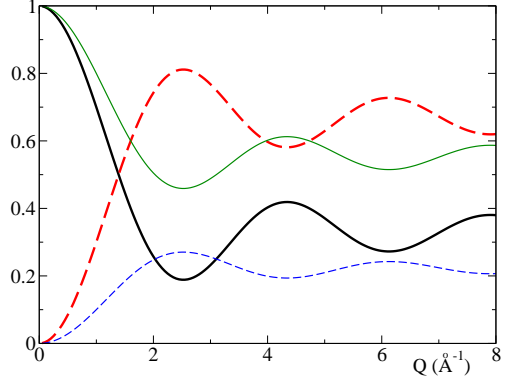


FIG. 3. Thick lines: $A(Q)$ (solid) and $1 - A(Q)$ (dashed) for methyl group classical hopping. Thin lines: $A(Q)$ (solid) and $(1 - A(Q))/2$ (dashed) for methyl group rotational tunnelling.

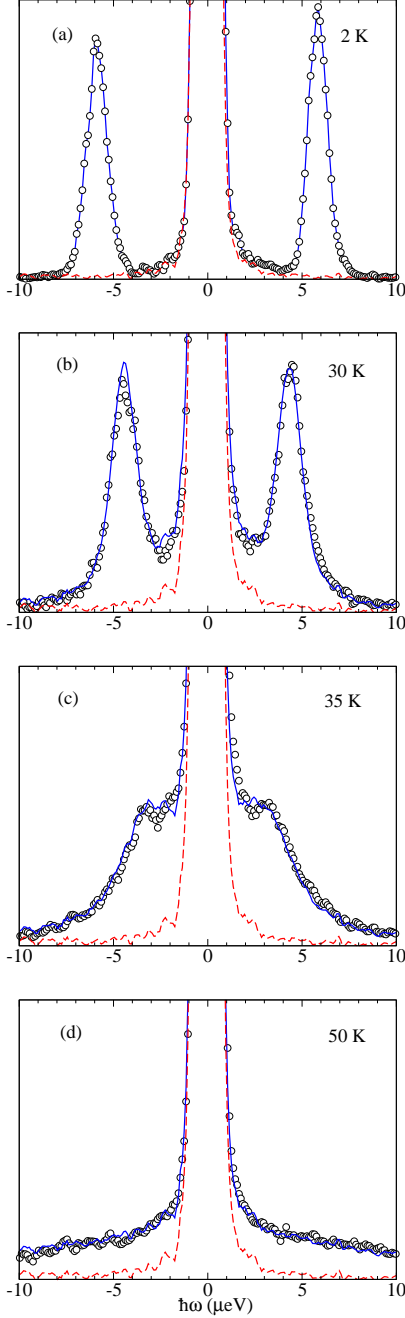


FIG. 4. Experimental spectra (circles) for methyl group dynamics in crystalline sodium acetate trihydrate. Solid lines are fits to the model for crystalline systems exposed in Section III. Dashed lines correspond to the experimental resolution. $Q = 1.8 \text{ \AA}^{-1}$. Scales (referred to the maximum): (a) 8%, (b)-(d) 5%.

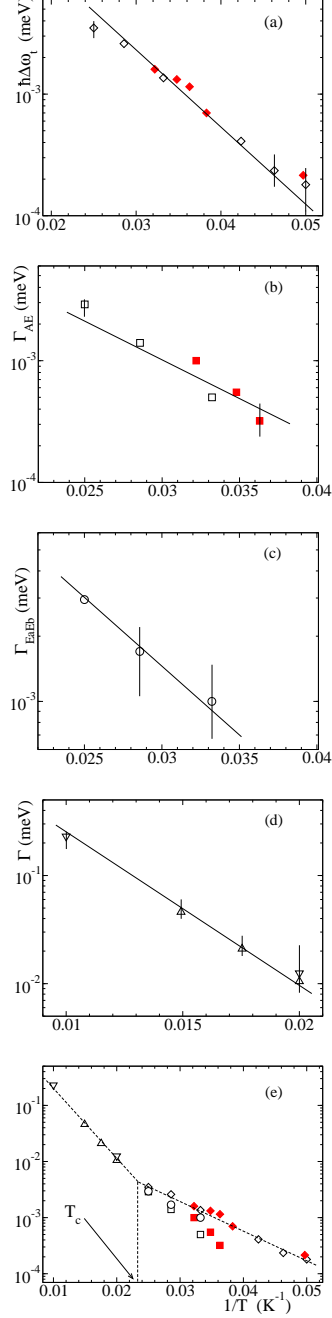


FIG. 5. Temperature dependence of the shift of the tunnelling frequency and of the crossover and classical Lorentzian HWHM for crystalline sodium acetate trihydrate. Solid lines in panels (a-d) are fits to respectively, Eqs.(18),(23),(24) and (15). Panel (e) shows all the data in a common frame. The arrow indicates the crossover temperature T_c . Dotted lines are a guide for the eyes.

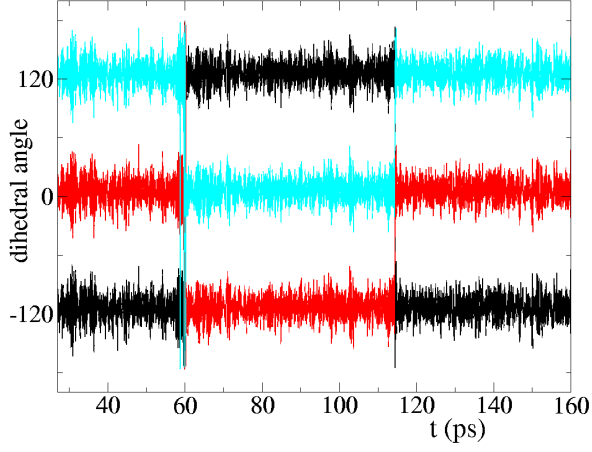


FIG. 6. Simulated time evolution of the orientation of a typical methyl group in polyisoprene at $T = 150$ K. Trajectories of different hydrogens are represented by different tones.

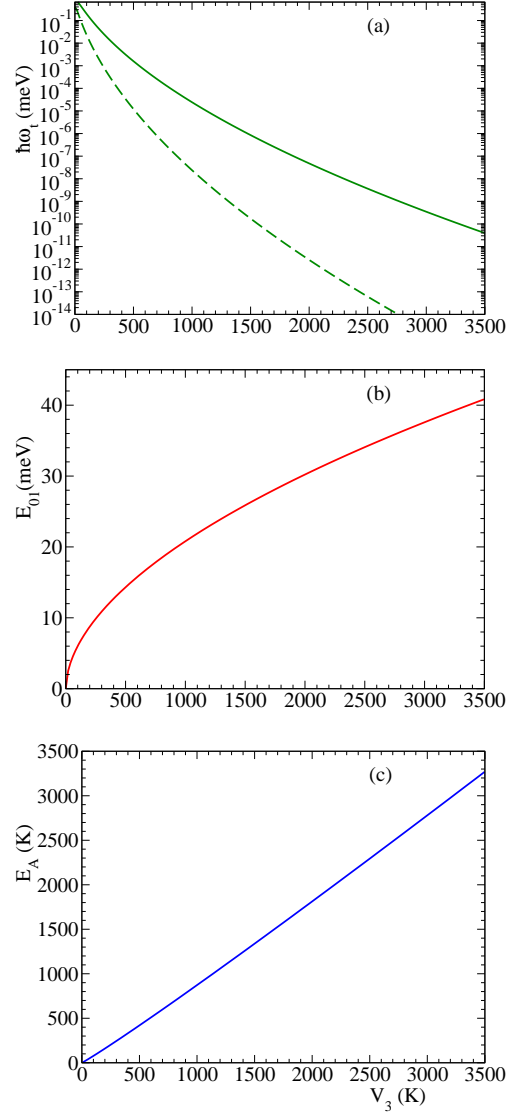


FIG. 7. Solid lines: dependence on the barrier height of the tunnelling frequency (a), first librational energy (b) and classical activation energy (c) for a protonated methyl group in a purely threefold potential. The dashed line in panel (a) corresponds to a deuterated methyl group.

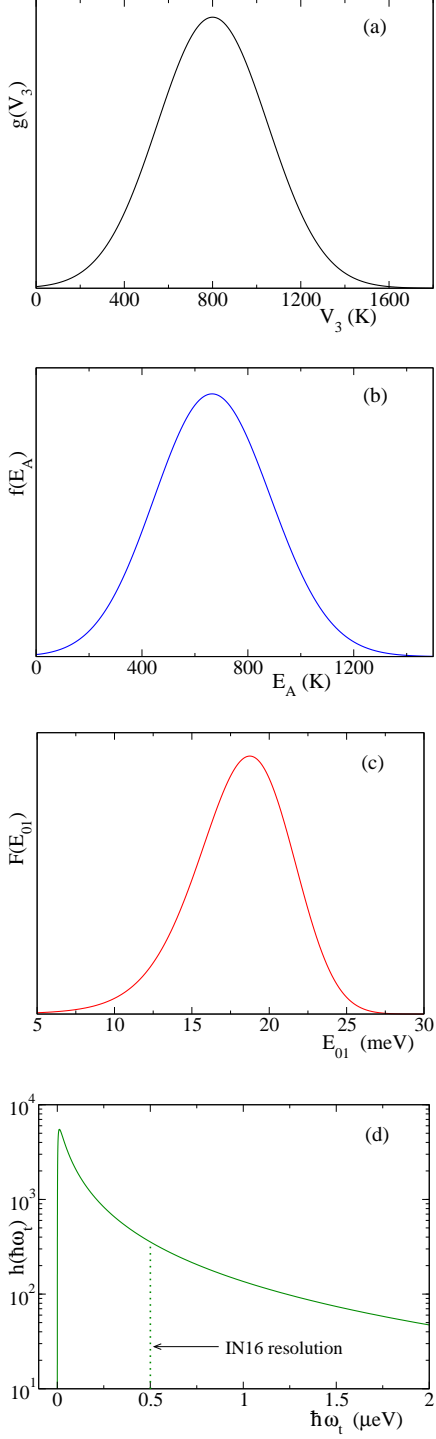


FIG. 8. Distributions $g(V_3)$, $f(E_A)$, $F(E_{01})$ and $h(\hbar\omega_t)$ for an average barrier $\langle V_3 \rangle = 800$ K and a standard deviation $\sigma_V = 250$ K.

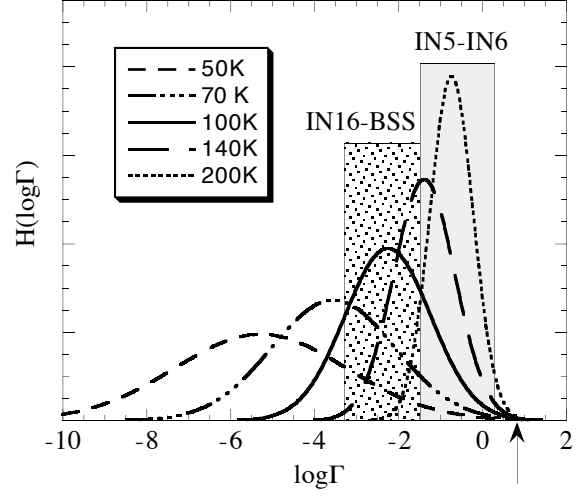


FIG. 9. Temperature dependence of the distribution $H(\log\Gamma)$, for the set of parameters $\langle V_3 \rangle = 800$ K, $\sigma_V = 250$ K and $\Gamma_\infty = 6$ meV. Γ is given in meV. The value of Γ_∞ is indicated by the arrow. Shaded areas correspond to the energy windows of some BS and TOF spectrometers.

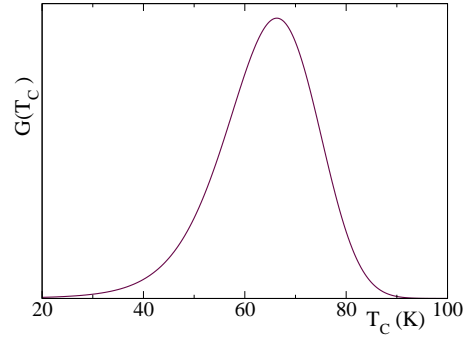


FIG. 10. Distribution of crossover temperatures $G(T_c)$, for the same set of parameters $\langle V_3 \rangle = 800$ K, $\sigma_V = 250$ K and $\Gamma_\infty = 6$ meV of Figs. 8 and 9.

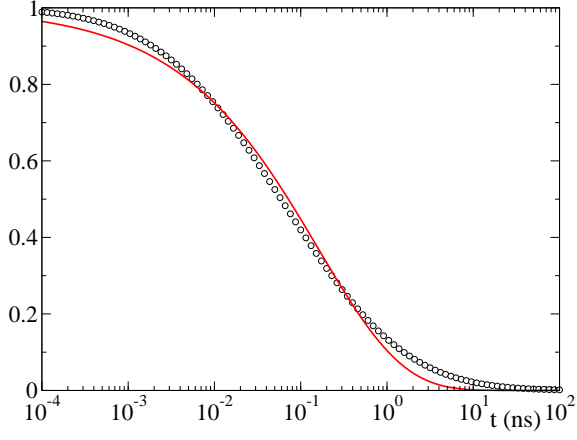


FIG. 11. Comparison between $\mathcal{F}(t)$ given by the RRDM expression (50), for parameters $\tau = 0.1$ ns and $\sigma = 1$ (circles), and a fit to a KWW function (solid line) in a wide dynamic range.

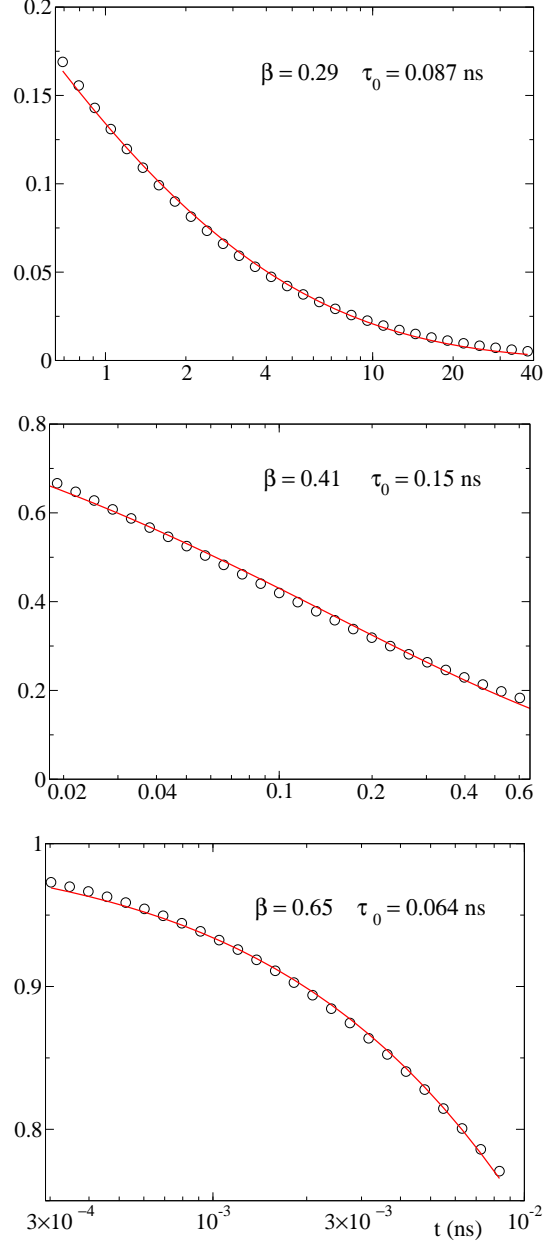


FIG. 12. As Fig. 11, but KWW fits are done in different narrow intervals covering, as in usual experimental conditions, 1-2 decades in time. The obtained values of β and τ_0 for the KWW description are shown.

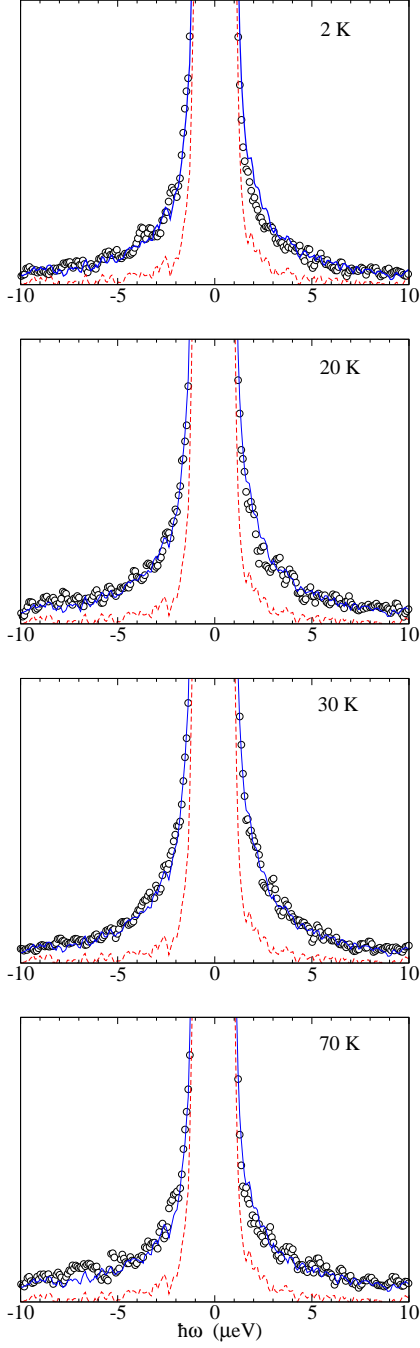


FIG. 13. IN16 spectra for PVAc at $Q = 1.8\text{\AA}^{-1}$ and different temperatures. Circles are experimental data. Solid lines correspond to the RRDM description. Dashed lines are the resolution function. The scale is a 5% of the maximum.

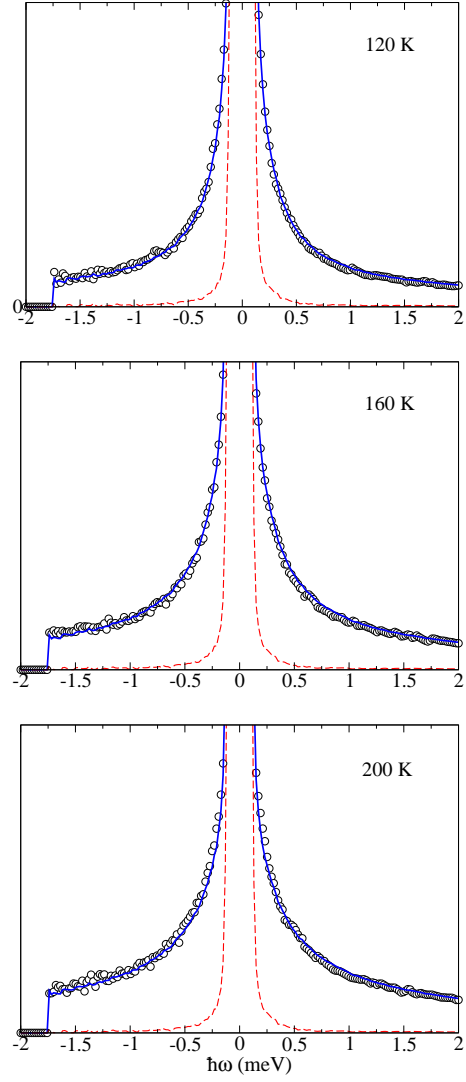


FIG. 14. IN6 spectra for PVAc at $Q = 1.5\text{\AA}^{-1}$ and different temperatures. Circles are experimental data. Solid lines correspond to the RRDM description. Dashed lines are the resolution function. The scale is a 3% of the maximum.

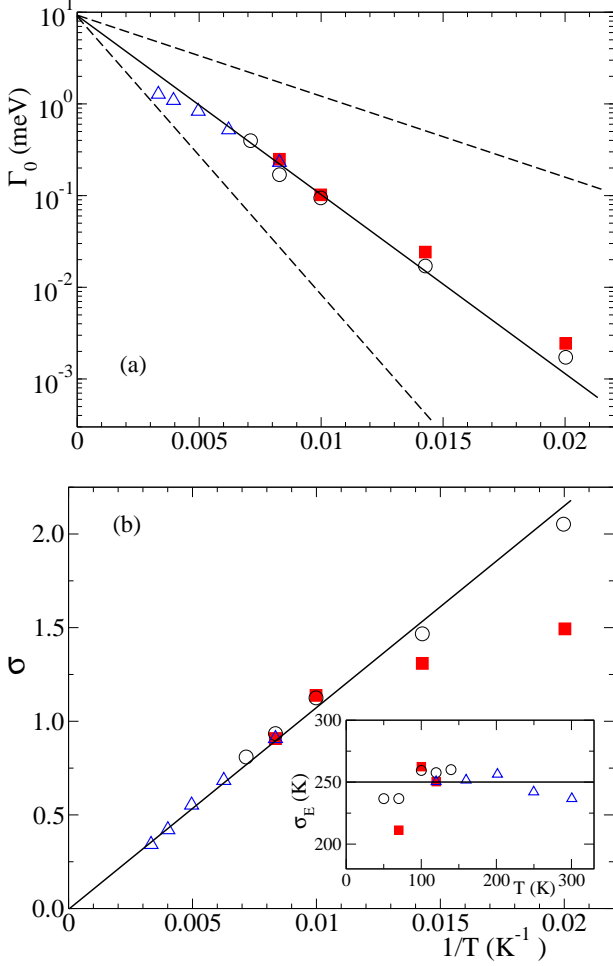


FIG. 15. Temperature dependence of Γ_0 (a) and σ (b) for PVAc. Different symbols indicate the different used spectrometers: IN16 (squares), IN5 (circles) and IN6 (triangles). Solid lines for Γ_0 and σ are respectively fits to Eqs. (45) and (46). The inset in panel (b) shows the values of σ_E obtained at each temperature from the corresponding values of $\sigma(T)$ by transformation through Eq. (46). The horizontal line corresponds to the value obtained by fitting the latter values to Eq. (46). Dashed lines in panel (a) correspond to $\Gamma = \Gamma_\infty \exp[-(\langle E_A \rangle \pm \sigma_E)/k_B T]$.

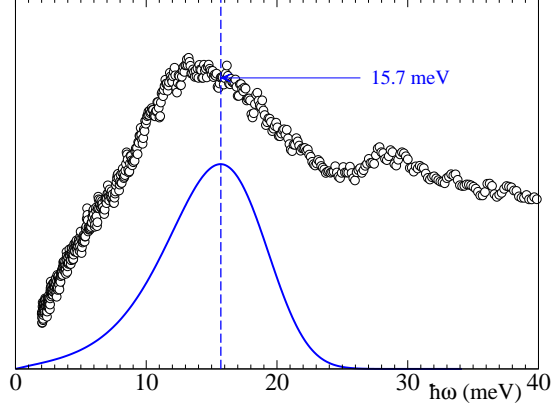


FIG. 16. Generalized VDOS (circles) for PVAc, measured at TOSCA at $T = 20$ K. The curve corresponds to the RRDM theoretical distribution $F(E_{01})$. The arrow indicates the maximum of the latter for comparison with experiment.

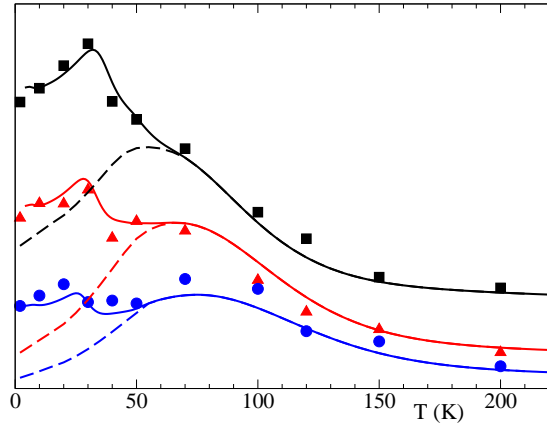


FIG. 17. Experimental integrated inelastic intensities for PVAc at $Q = 1.8 \text{ \AA}^{-1}$ in the intervals 1-2.5 μeV (squares), 2.5-6 μeV (triangles) and 6-10 μeV (circles). Solid lines correspond to the theoretical description by the general version of the RRDM. Dashed lines are an extrapolation of the classical limit of the RRDM to low temperatures.

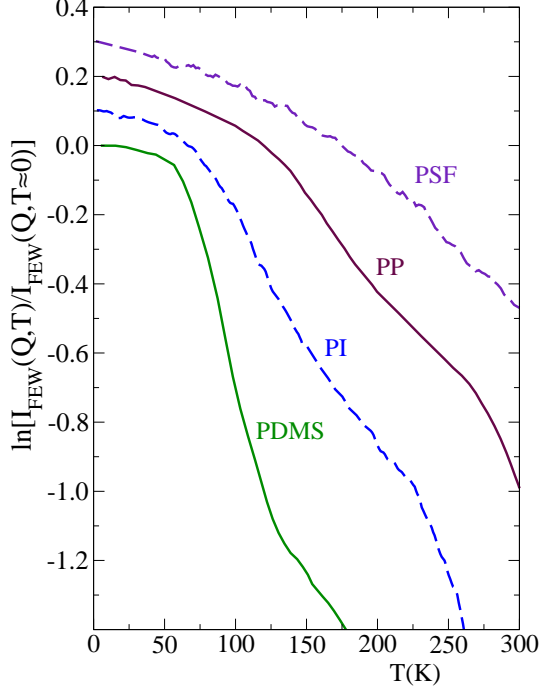


FIG. 18. Temperature dependence, for several polymers, of $\ln[I_{FEW}(Q,T)/I_{FEW}(Q,T \approx 0)]$, with $I_{FEW}(Q,T)$ the FEW intensity, measured in BS spectrometers. For clarity, data are consecutively shifted by 0.1. $Q = 1.8 \text{ \AA}^{-1}$ for PDMS and PSF; $Q = 1.95 \text{ \AA}^{-1}$ for PI and atactic PP.

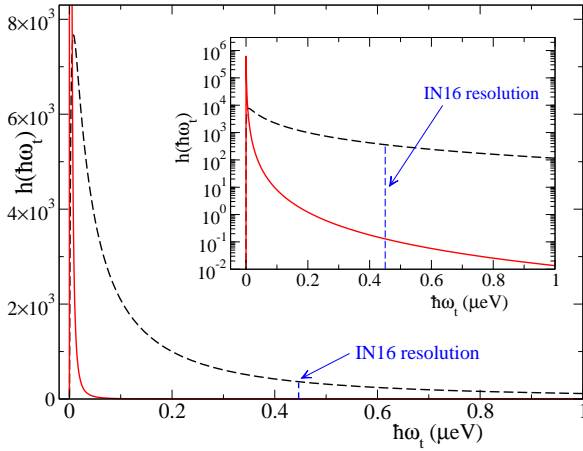


FIG. 19. Distribution of tunnelling frequencies for PMMA-d5 (dashed line), and PMMA-d8 (solid line). The inset shows both distributions in logarithmic scale.

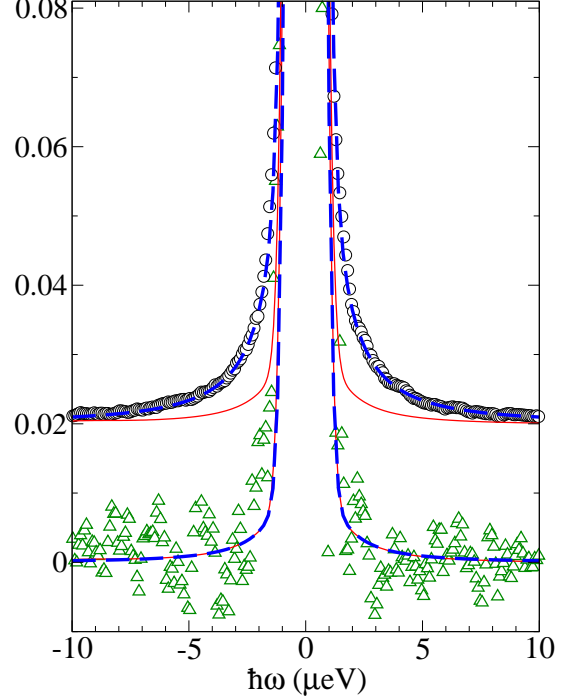


FIG. 20. Methyl group incoherent contribution, $S_{inc}^{MG}(Q, \omega)$, normalized to unity, for PMMA-d5 (circles) and PMMA-d8 (triangles) at $T = 2 \text{ K}$ and $Q = 1.8 \text{ \AA}^{-1}$. Dashed lines correspond to the description by the tunnelling limit of the RRDM. Solid lines correspond to the resolution function. Data for PMMA-d5 are shifted by 0.02 for clarity.

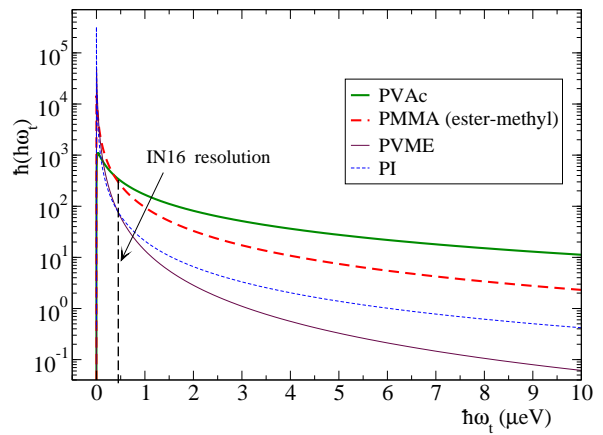


FIG. 21. Distribution of tunnelling frequencies for several polymers, as derived from the RRDM analysis of hopping and/or librational data.

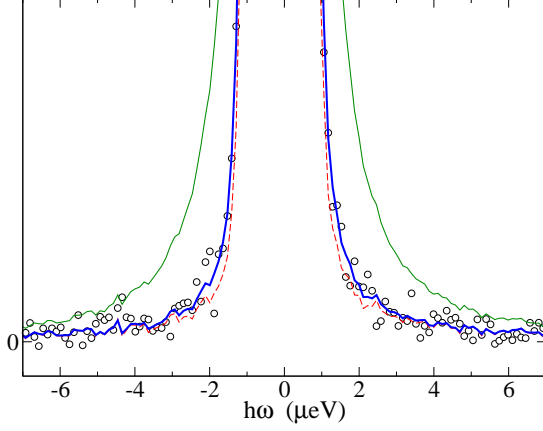


FIG. 22. Circles: Experimental spectrum at $T = 2$ K for PDMS. Thick and thin solid lines correspond to the theoretical spectra calculated respectively from the RRDM parameters reported in Refs. [89] and [93]. The dashed line is the resolution function. The scale is a 3 % of the maximum.

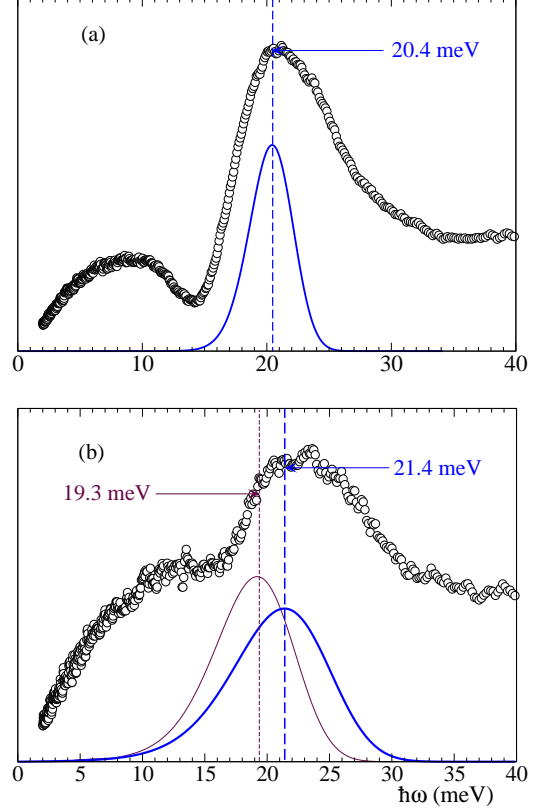


FIG. 23. Generalized VDOS (circles) measured at TOSCA, and RRDM theoretical distributions $F(E_{01})$ (solid lines). All data are obtained at $T = 20$ K. (a): PDMS (b): PMMA-d5. Arrows indicate the maxima of the theoretical $F(E_{01})$ for comparison with experiment. In panel (b), the thin line corresponds to a purely three-fold approximation, while the thick line corresponds to a sixfold correction $V_6/V_3 = 0.11$ (see text).

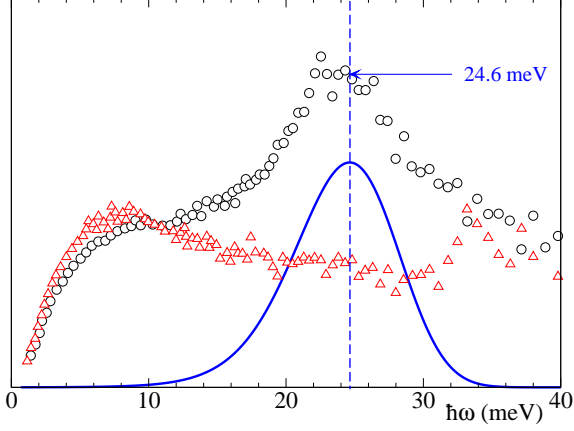


FIG. 24. Generalized VDOS for PI measured at IN6. $T = 140$ K. Circles: PI-d5 (deuterated main chain - protonated methyl group). Triangles: PI-d3 (protonated main chain - deuterated methyl group). Curve: RRDM theoretical distribution $F(E_{01})$. The arrow indicates the maximum of the latter for comparison with experiment.

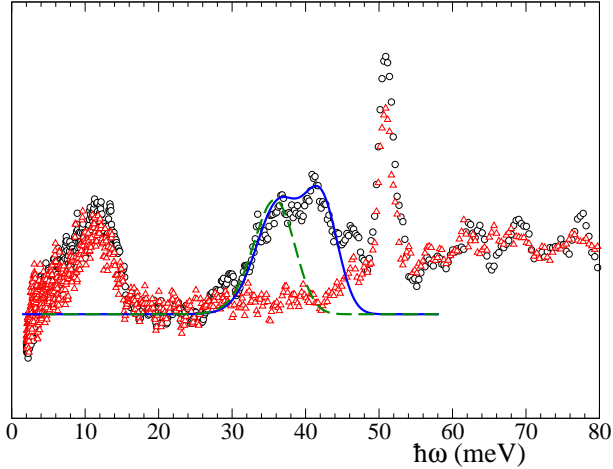


FIG. 25. Generalized VDOS for PSF measured at TOSCA. $T = 20$ K. Circles: fully protonated sample. Triangles: deuterated methyl group. Curves: RRDM theoretical distribution $F(E_{01})$ for a single-particle approach (dashed) and for an additional methyl-methyl coupling interaction (solid, see text).

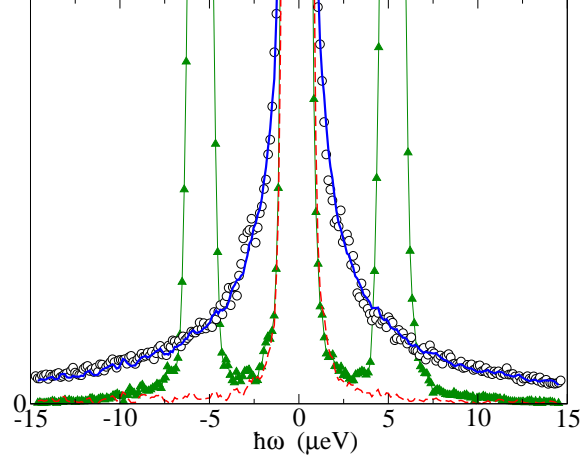


FIG. 26. Symbols: Experimental spectra for a same sample of sodium acetate trihydrate in the crystalline (triangles) and glassy (circles) state at $T = 2$ K and $Q = 1.8 \text{ \AA}^{-1}$. The thick solid line is the RRDM theoretical function. The thin solid line is a guide for the eyes. The dashed line is the resolution function. Scale: 3% of the maximum.

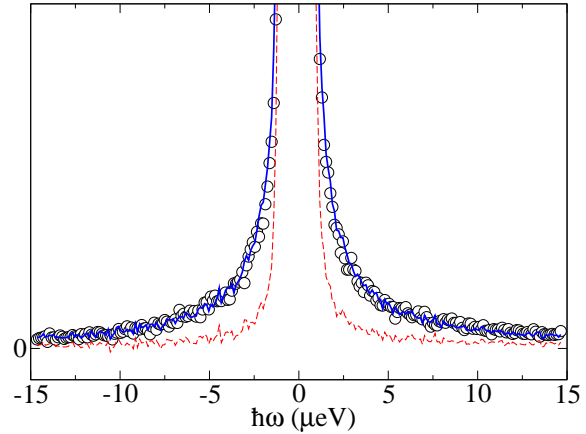


FIG. 27. Circles: Experimental tunnelling spectrum at $T = 2$ K and $Q = 1.8 \text{ \AA}^{-1}$ for tri(vinyl acetate). Solid line: Theoretical spectrum calculated from the RRDM parameters for PVAc. The dashed line is the resolution function. Scale: 3% of the maximum.

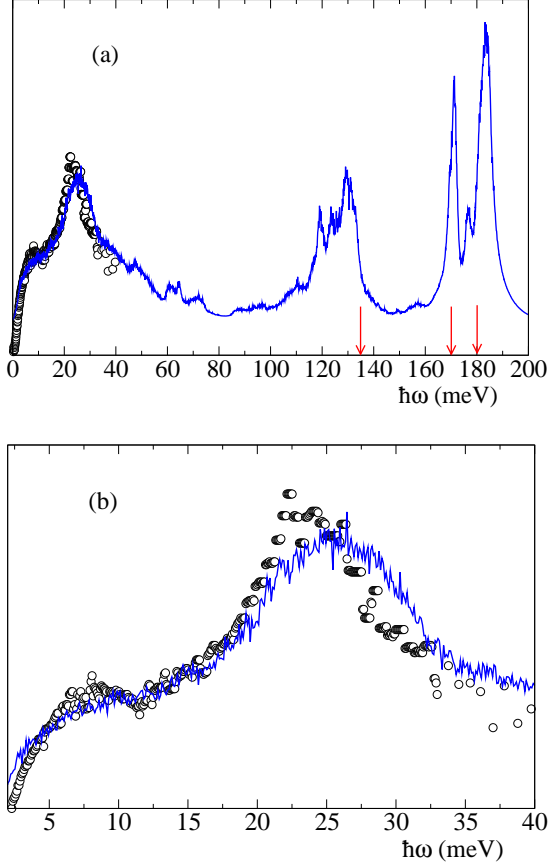


FIG. 28. Generalized VDOS obtained for PI-d5 by MDS (solid line), and by INS (circles). Arrows in panel (a) indicate the position of infrared bands. Panel (b) is an amplification in the energy range around the librational peak.

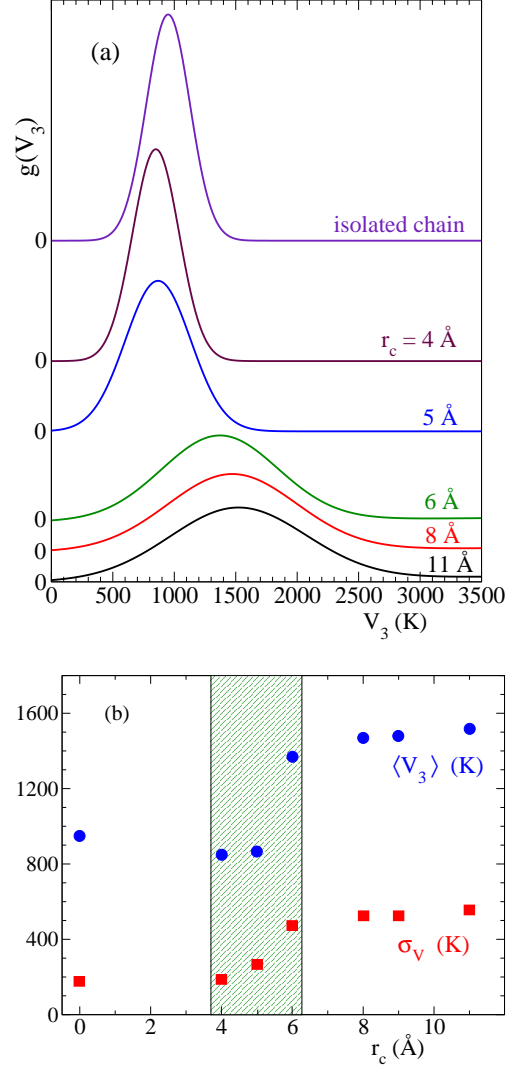


FIG. 29. Panel (a): Effect of the cutoff radius, r_c , for the nonbond interactions on the distribution of potential barriers for methyl group reorientation in PI. Panel (b) shows the evolution with r_c of the average potential barrier $\langle V_3 \rangle$ and the standard deviation σ_V . The shadowed area corresponds to the range of inter-chain distances.

	H	D	C	O
σ_{inc}	80.3	2.0	0.0	0.0
σ_{coh}	1.8	5.6	5.5	4.2

TABLE I. Scattering cross-sections of the most abundant nuclei in polymers. Values are given in barn (1 barn = 10^{-24} cm $^{-2}$).

	$\langle E_A \rangle$ (K)	σ_E (K)	Γ_∞ (meV)	$\langle V_3 \rangle$ (K)	σ_V (K)	E_{01}^{max} (meV)
PVME [25,115]	1010	276	7.8			
PVAc [31,33,89,146]	445	253	9.1	534	274	14.4
PI [92,147]	1170	353	62.1	1364	376	23.4
PDMS						
[89,146]	842	144	18.5	997	155	21.2
[93] (*)	602	132	0.63			
PEP [111]	1288	162	1.6			
PP						
atactic [90,145]	1744	421	28.8	1995	448	30.0
isotactic [144]						28.5
head-to-head [111,145]	1242 (§)	197 (§)	1.4			28.0
DMB [124]	842	361	40			
DHMS [124]	1071	385	40			
PSF [149]	2553	396	4.1	2727 ; $W_3^c = 522$	406	36.7, 41.6 (†)
PH [149]	2553	373	8.3	2727 ; $W_3^c = 522$	383	36.7, 41.6 (†)
PC [149]	2553	379	10.4	2727 ; $W_3^c = 522$	390	36.7, 41.6 (†)
PMMA (ester-methyl)						
syndiotactic [32,34]	710	241	4.8	820 ; $\langle V_6 \rangle = 90$	265	22.4
S1: (s:i:h) = (50:10:40) [91]	529	192	1.5			
blend isotactic/S1						
non-sc (i-methyl) [91]	770	313	4.8			
sc (i-methyl) [91]	686	205	2.8			
sc (S1-methyl) [91]	553	180	1.5			
PMMA (α -methyl)						
isotactic [17]						37.2
syndiotactic [17]						44.6
P α MS						
syndiotactic [17]						47.1
atactic [17]						47.1
head-to-head [17]						37.2
PPO [16,128]	1684 (‡)					28.3
PIB [145,147,148]						40.0

blend PVME/PS			
(65:35) [115]	1010	278	7.8
(20:80) [115]	1010	354	7.8
blend hh-PP/PEP			
(50:50; hh-PP-methyl) [111]	1242	197	1.4
n-hexatriacontane			
Mon (single-layered) [150]			30.0
Orth II (double-layered) [150]			29.4

TABLE II. Values of the RRDM parameters for the polymers investigated so far by neutron scattering techniques. E_A , σ_E and Γ_∞ are obtained from the analysis of high temperature data. Typical error bars are about a 10 % for the two formers and a 30 % for the latter. E_{01}^{max} denotes the maximum of the experimental librational peak. The parameters $\langle V_3 \rangle$ and σ_V of the barrier distribution $g(V_3)$ are given in the cases where the quantities E_A , σ_E and E_{01}^{max} are known, and a good correspondence between them is possible by assuming a purely threefold potential. In the cases of PVAc and syndiotactic (*s*) PMMA also the tunnelling and crossover regimes have been investigated. For PVAc a good description of the latter is possible with the given RRDM parameters, but for *s*-PMMA sixfold corrections with ratio $V_6/V_3 = 0.11$ are necessary (see Section VI). $\langle V_6 \rangle$ is indicated. In the case of PSF, PH and PC, a non-distributed coupling term is necessary to reproduce the librational double-peak (see Section VI). The coupling term W_c is indicated. For the systems where hopping or librational data are absent, there is no sufficient information to determine the shape of the potential, and the parameters of $g(V_3)$ are not given.

(*): These parameters, obtained from an analysis of hopping data, are incompatible with both the experimental librational peak and the tunnelling spectrum (see Section VI).

(§): In a purely threefold approach, these parameters provide a theoretical librational maximum of ≈ 26 meV, close but not fully satisfactory with the experimental value (see Section VII).

(†): Double-peak structure.

(‡): The standard deviation σ_E is not reported. In a threefold approach, the corresponding librational energy for the given $\langle E_A \rangle$ is 29.7 meV, to be compared with the experimental maximum.